HEAD KINEMATICS AND PENETRATION THROUGH DAMP GRANULAR MEDIA BY A ROBOTIC SQUAMATE ANALOGUE

A Dissertation

Presented to

The Graduate Faculty of the University of Akron

In Partial Fulfillment of the Requirements for the Degree of

Doctor of Philosophy

Charles Samuel Edwards

December, 2024

HEAD KINEMATICS AND PENETRATION THROUGH DAMP GRANULAR MEDIA BY A ROBOTIC SQUAMATE ANALOGUE

Charles Samuel Edwards

Dissertation

Approved:

Advisor
Dr. Henry C. Astley

Committee Member
Dr. Petra Gruber

Committee Member
Dr. Rachel Olson

Committee Member
Dr. Julian Tao

Committee Member
Dr. Philip Bergmann

Committee Member
Dr. Peter Niewiarowski

Accepted:

Interim Chair
Dr. Jordan M. Renna

Dean of the Buchtel College of Arts and Sciences
Dr. Mitchell S. McKinney

Interim Dean of the Graduate School
Dr. Gwen Price

Date

ABSTRACT

In this thesis, a novel type of hydraulically-actuated robophysical model was used to test hypotheses concerning the relationship between head kinematics and the force and work required for burrowing through damp granular media by amphisbaenians, a clade of mostly limbless, burrowing squamates. The design of the robot was intended to mimic a simplified, limbless body plan similar to that found among burrowing squamates, having an extendable cylindrical shaft and an oscillating, bullet-shaped head. Forces and work of an actuated head and shaft were compared while forward penetration occurred simultaneously with head oscillation amplitudes of 5, 10, and 15 degrees from a centerline, at a ratio of 1 and 2 oscillations per push distance, and compared to a control group with no head movement. An intermittent push strategy was also investigated in which the oscillation of the head was decoupled from the forward penetration of the shaft so that the machine alternated between a forward push and a head oscillation phase. The distance traveled by the robot between each oscillation phase was varied, and force and work were observed for distances of 2cm, 4cm, and 8cm between each oscillation phase, with either 1 or 2 head oscillations per phase. The peak force experienced, and the total work done by the shaft decreased with a 15 degree head oscillation amplitude, but any reduction in these variables is more than offset by the increase in force and work required to rotate the head. Amphisbaenians are a relatively diverse clade, well adapted to subterranean locomotion, but despite their diversity they are understudied. Understanding the significance of head kinematics could be informative for bioinspired digging machines, and could shed light on the biology of the animals. Meanwhile, the suitability of crushed, expanded perlite as a proxy for other damp granular media in laboratory experiments was explored, with implications for similar experiments as well as interpreting data from burrowers across different substrates.

DEDICATION

To Paul, Violet, Florence

and

Grandad

ACKNOWLEDGEMENTS

I would like to acknowledge the help of many colleagues, family members, and friends during this process. This includes, but is not limited to:

My brother, Dr. Abraham Edwards (who made me think that if *he* could get a PhD, then I could at least give it a shot). Thanks to my mother Dr. Lucinda George and my grandmother Margaret George for much support along the way. Also to the undergraduate students that worked with me: Jacob Newell, Sarvesh Sudhaharan, Sophie Kheder and Ryan Hogan. My friends and colleagues from the Astley lab have been a big help – including Dr. Kaelyn Gamel, Dr. Colleen Unsworth, Kelsey Garner, Hope Zimmerman and Jacob Sherman. To my coworkers at Allegheny Restoration and Builders in Neffs, Ohio, and especially Jon Smith, who taught me shop techniques and ways of thinking about practical problems that proved to be a big help with research. To my thesis committee members: Dr. Philip Bergmann, Dr. Julian Tao, Dr. Rachel Olsen, Dr. Petra Gruber, Dr. Peter Niewiarowski, and my advisor Dr. Henry Astley. To Dueber Church in Canton Ohio and the Monday night Foundry Group whose prayers played a pivotal role in the completion of my research. And finally, the One to Whom all credit is due... “Unless the Lord builds the house, the builders labor in vain” (Psalm 127:1).

TABLE OF CONTENTS

LIST OF FIGURES

LIST OF TABLES

CHAPTER I

INTRODUCTION

The study of animal locomotion has predominantly focused on the mechanics of flying, swimming, and locomotion over land, leading to significant advances in our understanding of these behaviors (Li et al., 2009;Li et al., 2013; Lopez-Arreguin & Montenegro, 2020; Nishikawa et al., 2007). This research has furthered our understanding of the mechanics of these types of locomotion, and has led to many useful, bio-inspired applications (Gao et al., 2019; Heydari et al., 2020; Mazouchova et al., 2013; Roberts et al., 2011). A large area of application is in robotics, as bioinspired robot designs have proven to be more efficient and maneuverable in general than non-bioinspired robots (Zhang and Gao, 2012). An area that is lagging in bioinspired locomotion is subterranean locomotion (including burrowing and tunnel building), and few burrowing machines exist for practical application that match the performance of living organisms (Aguilar et al., 2016; Naclerio et al., 2021).

Part of the difficulty is that locomotion through granular media is relatively poorly understood (Aguilar et al., 2016; Zhang & Goldman, 2014) as are the mechanics of tunnel formation (Herrel et al., 2021). A better understanding and application of the principles of excavation and movement within granular media can be relevant to a wide variety of fields including construction, resource extraction, interplanetary exploration, and search and rescue (Isava & Winter, 2016; Kubota et al., 2007; Sadeghi et al., 2017; Zhang & Gao, 2012). Thus, despite the challenges, bionispired designs have been explored based on a variety of species that inhabit and successfully move through subterranean environments. This has included a wide range of taxa, such as annelid worms (Calderón et al., 2019; Kubota et al., 2007; Ortiz et al., 2019; Zagal et al., 2012), bivalves (Germann et al., 2011; Isava & Winter, 2016; Winter et al., 2014), insects (Pitcher & Gao, 2017), rodents (Zhang & Gao, 2012), and plant seeds, roots, and vines (Coad et al., 2019; Mishra et al., 2018; Naclerio et al., 2021; Sadeghi et al., 2017; Tang et al., 2024; Tang & Tao, 2022). Among squamates, successful model organisms for machine design have included the sandfish lizard (*Scincus scincus*) (Maladen et al., 2011), and amphisbaenians (Tang et al., 2024; Xue et al., 2024).

However, subterranean locomotion through granular media remains a challenging area of study. The mechanics involved are still being explored and the underlying mathematics are still not fully understood (Agarwal et al., 2023; Schiebel et al., 2020; Naclerio et al, 2021). Much useful work is being done to deepen our understanding of this subject, but research has more often focused on dry granular media than on damp (Mitarai et al., 2006; Sharpe et al. 2015). The distinction is an important one. Particle interactions in dry granular media are short-range (except in compression) and are mainly influenced by friction and inelastic collisions (Mitarai & Nori, 2006). Capillary effects and other effects of surface tension mean that the addition of water to a granular substrate will increase the cohesion between grains (Hornbaker et al., 1997; Dorgan, 2010; Sharpe et al. 2015), and this cohesiveness becomes a dominating characteristic of the mechanics

(Mitarai & Nori, 2006). This increased cohesiveness with the addition of water, however, holds true only to a point – when the media is saturated it enters a "slurry" state, capillary action no longer holds the grains together, and the media loses the cohesive interaction between particles (Mitarai & Nori, 2006; Dorgan, 2010; Sharpe et al., 2015). Thus the mechanics of damp granular media can behave quite differently depending on the moisture content (Dorgan, 2015; Hosoi & Goldman, 2015), and the mechanics of saturated granular media are different still than either dry or damp media (Sharpe et al. 2015).

There are some general trends that can be observed in damp granular media. Before reaching the saturated slurry state, damp granular media shows plasticity, an increase in shear strength, and history dependence as a result of the moisture content (Sharpe et al 2015). Penetration resistance is also sensitive to both moisture content and compaction in cohesive soils (Sharpe et al. 2015). Dry sand can be made to flow when a force is applied, which allows some organisms to adopt strategies analogous to those for moving through a low Reynold's number fluid (Hosoi & Goldman, 2015). Locomotors moving through damp granular media are unable to use some of the strategies employed by those in dry media, such as fluidization, but the cohesiveness of the substrate allows them to use strategies unavailable to animals in dry media, such as the construction of tunnels or burrows that will stay in place once created (Sharpe et al 2015; Shinoda et al., 2018).

The lack of research involving damp granular media may be due, in part, to the experimental challenges that this media presents, especially in regards to numerical approximations (Zhang and Goldman 2014) and the preparation of repeatable trials for laboratory experiments (Sharpe et al., 2015). For example, the mechanics of locomotion through dry granular media can at least be approximated through a technique such as resistive force theory (Zhang and Goldman 2014). Here, the object in question is computationally divided into infinitesimal segments and the thrust and drag experienced by each segment can be summed to approximate the forces acting on the locomotor as a whole (Zhang and Goldman 2014). This works in dry granular media, because they lack cohesion and are not history dependent, i.e. the forces experienced are not changed by past movements through a given location. Therefore, behavior of one segment does not affect the forces acting on the following segments (Zhang and Goldman 2014) (at least when submerged, this is not true at the surface (Mazouchova et al., 2013). An undulating body or a rotating head can thus be approximated through the integration of forces across all segments if movement is taking place at a sufficient depth below the surface (Zhang and Goldman 2014). Because the addition of water to granular media leads to cohesion between particles (Sharpe et al 2015), and history dependence becomes an issue, influencing the forces encountered by segments during locomotion through the media. Now, trailing segments will encounter the surrounding media in a different way depending on the movement of the leading segment.

From the logistical standpoint, it can be difficult to prepare repeatable laboratory trials for testing damp granular media. Technology such as fluidized air beds are an immense help in performing repeated experiments involving locomotors in dry media, because the testing area can be automatically reset after each trial (Astley et al., 2020; Li et al., 2009, 2012; Maladen et al., 2009). However, this method cannot be used for damp media, due to this media's inability to fluidize. Methods to deposit homogenous batches of media have been developed (see Sharpe et al. 2015), but these methods still require the testing area to be emptied and refilled in preparation for each individual trial. This results in a labor intensive and time-consuming process. Additionally, the high forces involved with penetration through damp granular media present challenges in designing a testing apparatus with readily available material. Penetration and drag force through wet sand, for example, can be as much as four times that of penetration through dry sand (Sharpe at al, 2015) and require forces that push the limits of the strongest commercially available resin for 3D printing. Meanwhile, individual sand grains (which are difficult to contain entirely) can cause damage to components such as gears, pistons, and circuit boards.

Other, less logistically problematic granular media can be used as a testing substrate, but little is known about the comparability of results obtained in differing media. This question of comparability is mirrored by an interesting question in the natural world, as granular substrates can differ widely between habitats, and penetration forces can vary depending on particle shape and size (Bergmann & Berry, 2021). Particle morphology is in turn dependent on the geological history of the particle formation (Cho et al., 2006), thus an organism burrowing in one location may face different mechanical constraints than the same organism burrowing in a different location with a different formation history.

Although challenging to study, damp granular media is not only a common substrate for terrestrial locomotion, it is more commonly encountered in terrestrial habitats than dry granular media (Sharpe et al. 2015). And while the methods developed for dry granular media make it an attractive area for laboratory study that has generated much useful data, the different mechanics mean that the results of experiments involving dry media cannot be assumed to apply to locomotion through damp. As a result, locomotion through damp granular media remains an open and attractive area for academic research and means of overcoming the logistical challenges are needed. In this thesis, crushed, expanded perlite is used as a testing substrate – a granular medium with a low density made from a heat-treated volcanic rock (Sodeyama et al., 1999). This medium requires far less force to move through than other commonly used substrates (such as sand) and is soft enough to minimize damage to the components of the machine.

Organisms that move through granular media have a diversity of kinematic strategies to help them locomote through this challenging substrate, and there is a diversity of strategies even among those of similar body plans inhabiting similar substrates (Sharpe et al., 2015; Gans, 1968). Movement strategies have been the subject of study in a variety of limbless, elongate burrowers (Herrel et al., 2011; Herrel & Measey, 2010; Hipsley et al., 2016; Hohl et al., 2014; Martín et al., 2013; Navas et al., 2004; Ducey et al., 1993). For example, research has examined the influence of compaction on soil choice, burrowing success, and burrowing time in caecilians (Ducey et al. 1993), and also on locomotion kinematics in caecilians (Herrel & Measey, 2010). Cinefluoroscopy has been used to examine the kinematics of two burrowing eel species in saturated sediment, determining maximum push forces and finding evidence to support the hypothesis that the head-first borrower's skull morphology is better adapted to head-first burrowing than that of a tail-first burrower (Herrel et al., 2011).

Of fossorial vertebrates, a large proportion of limbless burrowers are represented by amphibians (notably the caecilians), and squamates. Except for a few aquatic species, Caecilians (represented by 198 known burrowing species) live in moist soils, due to their need to keep their skin moist. In hard soils, burrowing squamates are represented by snake species belonging to the families of Uropeltidae (represented by 56 known species), Xenopeltidae (represented by 2 species) and Scolecophidia (457 species); lizards of the genus *Anniella* (6 species) and family Dibamidae (23 species); and nearly the entire suborder of amphisbaenia (201 species) (Augé, 2012; Gans, 1978; Hohl et al., 2014; ITIS, 2024). Thus, while amphisbaenians are not the most speciose group, they represent a large proportion of the successful vertebrate burrowers in hard soils specifically, and of burrowing squamates in general. Moreover, amphisbaenians show a diversity in habitat, and are known for their diversity of head shapes (Kearney, 2003), some of which show similarities that are not monophyletic (Augé, 2012; Gans, 1978), suggesting important hypotheses concerning the head shape and evolution of this group (Navas et al. 2004). Additionally, amphisbaenians are very successful in moving through compact soils, invading niches that are inaccessible to other reptiles (Gans, 1968) making them an attractive model for bioinspired engineering.

Nonetheless, in proportion to their diversity, amphisbaenians are underrepresented in the literature, and are "arguably one of the least studied squamate lineages" (Kearny 2003, p.59). This is due, part, to the extreme difficulty of finding them and keeping them alive in captivity (Hawkins et al., 2022; Navas et al., 2004). However, distinctive head geometries and relative simplicity of movement of some species are advantages in constructing robophysical models that can allow for testing specific hypotheses that might otherwise be difficult to test concerning kinematics and morphology. For example, understanding morphology and behavior could help to suggest which species are more basal and which are more specialized, possibly helping with problematic phylogenies for clades such as amphisbaenia (Kearney 2003). Meanwhile, as representative of burrowing squamates, they can be instructive to bioinspired engineering for applications such as search and rescue (Coad et al., 2019), archaeology (Knudson, 1999; Musteata, 2015), or other applications where minimal impact to the immediate surroundings are desirable. While many organisms have been under investigation as biological role models for burrowing, especially promising for these specific areas of application include small, limbless organisms that are capable of movement by substrate rearrangement or packing, rather than bulk excavation (Dorgan 2015; Dorgan & Daltorio, 2023). This includes worms, plant roots, and burrowing squamates as model organisms. For example, soft expanding segments can mimic the peristalsis used by annelid worms, allowing for limbless movement in confined spaces (Calderón et al., 2019; Kubota et al., 2007; Ortiz et al., 2019; Liu et al., 2019). A plant root inspired robot was developed that functions through a process of self-printing through soil - similar to the expansion of plant roots at the tip (Sadeghi et al., 2017). While these designs hold promise, soft materials lack the strength of rigid materials and worms have difficulty with horizontal burrowing in nature (Dorgan and Daltorio, 2023). An expansion-by-printing root design leaves material behind and thus would be problematic for situations where a tunnel is needed (such as cable-laying) or where minimal changes to the environment are desired (such as archaeology).

Because of their relatively high representation among vertebrate burrowers, their unusual diversity of head shapes, their potential as biological role models for engineering, and their conduciveness to robophyiscal modelling, amphisbaenians will be a focus of this thesis. Amphisbaenians are generally found in moist substrates, potentially due to the water permeability of their skin and the ability of moist substrates to be formed into tunnels (Gans, 1968). Once the tunnel has been constructed, the energy required to move underground through this excavation is decreased, as is the energy required for respiration as the body of the animal would otherwise have to push against the substrate while breathing (Gans, 1968). Like most burrowing organisms, Amphisbaenians appear to have developed several adaptations to aid in subterranean locomotion, including limblessness (except for Bipes, in which two tiny forelimbs are retained), elongation, and a robust skull (Gans 1968) – adaptations that are often associated with fossoriality in other organisms as well (Bergmann et al., 2020; Deufel, 2017; Morinaga & Bergmann, 2020). Additionally, amphisbaenians have developed distinct kinematic strategies to aid in locomotion and tunnel formation (Fig. 1). Interestingly, these kinematic strategies are correlated to specific skull shapes, resulting in four specific patterns (Gans 1968) (Fig. 1).

The first and most widely distributed pattern is associated with a generalized rounded or bullet-shaped skull (Gans 1968). This pattern involves an irregular repetition of apparently random movements, in which the head moves either during forward penetration or intermittently between the forward pushes (Gans 1968). A second pattern involves a “corkscrew” type of motion that combines a rotational twist with a simultaneous forward penetration movement (Gans 1968) (Fig. 1F). This is correlated with sharp edges on either side of the snout, which shave off material from the surrounding media as the animal moves (Gans 1968) (Fig. 1C). This pattern/morphology combination appears to be advantageous in sand and sandy soils and allows for rapid burial in hot and dry environments to access a cooler and moister substrate (Gans 1968). The corkscrew pattern is found among members of the family Trogonophidae, which inhabit sandy soils in north Africa and the Arabian peninsula (Gans 1968). A third pattern involves a side-to-side rotation of the head, in conjunction with the forward penetration movement (Fig. 1E) (Gans 1968). In this case, the skull is flattened laterally, so that the head resembles a wedge shape (this morphology has also been termed “keel snouted”, Fig. 1B) (Gans 1968). A third pattern of morphology and kinematic strategy is the “shovel snouted” type of amphisbaenian (Fig. 1A), which pushes (or possibly rams) a dorsally flattened shovel-like head into the substrate and then lifts it to pack the media into the ceiling (simultaneously flattening the floor with its ventral side – Fig. 1D) (Gans 1968). The keel and shovel snouted types are found in more compact and deeper soils than Trogonophids or amphisbaenians with more generalized morphologies and kinematics (Gans 1968). Trogonophids, shovel snouted amphisbaenians, and keel snouted amphisbaenians generally are not found in the same geographical areas, while the range of the generalized types can be overlap with any of the three others (Gans 1968).

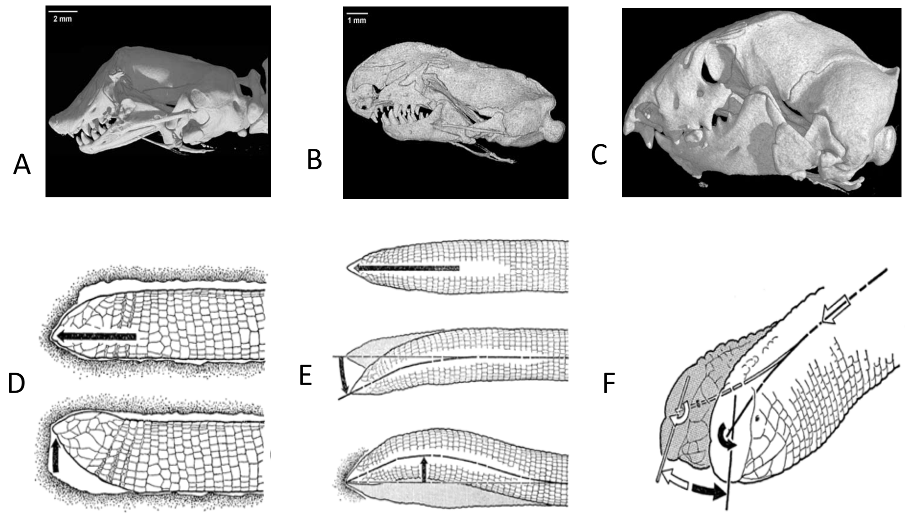

Figure 1: Skull morphology and burrowing strategy of (a) shovel-snouted [lateral view], (b) keel-snouted [dorsal view], and (c) Trogonophidae amphisbaenians. Skull images are from Digimorph.org. Burrowing sketches are from Gans 1968.

While amphisbaenians may exhibit head movement either with or separate from the forward push, Gans (1968) suggests that the decoupling of the head oscillation and the forward penetration results in an increased mechanical efficiency for burrowing. From a mathematical standpoint, intermittent ramming motions, as opposed to a single continuous push, should be advantageous due to the fact that the force the animal applies to the substrate is equal to its mass times its acceleration – thus multiple short bursts of acceleration result in a higher force than a continuous push (Gans, 1960). Both of these suggestions are, however, hypothetical, as there is no published data comparing these strategies.

Some data has been obtained concerning the locomotion kinematics of burrowing amphisbaenians. For example, Hohl et al. (2014) was able to quantify burrowing speed (approximately 0.25 cm/s) and cycle frequency (approximately 0.53 cycles per second), for *Leposternon microcephalum* of an average length of 33.83cm and an average weight of 50.81g. (Hohl et al., 2014). Navas et al. (2004) was able to record maximum push forces in *L. microcephalum,* recording maximum forces up to 24N for animals measuring 40.9cm in average length, 0.99cm in average head width, and weighing an average of 5.73g. Morphology and physiology of skull and muscles have also been examined (see, for example, Hipsley 2016 and Navas et al., 2004). However, the more complex relationship between head oscillation patterns during locomotion on the forces experienced by burrowers remains largely unknown. An exception is an experimental study conducted by Sharpe et al. (2015) in which observation of the burrowing behavior of the Ocellated skink (*Chalcides ocellatus*) (Fig. 2) prompted a mechanical simulation that looked at drag forces following the rotation of a cylindrical rod (Fig. 2). Ocellated skinks employ a side-to-side head rotation that is simultaneous with forward penetration (Fig. 2) (Sharpe et al. 2015). One hypothesis for this behavior is that it weakens the resistance of the media and thereby decreases the force needed to penetrate (Sharpe et al. 2015; Hosoi and Goldman 2015). Sharpe et al (2015) found that a side-to-side rotation of 20-degree amplitude (from the centerline), decoupled from forward penetration, initially

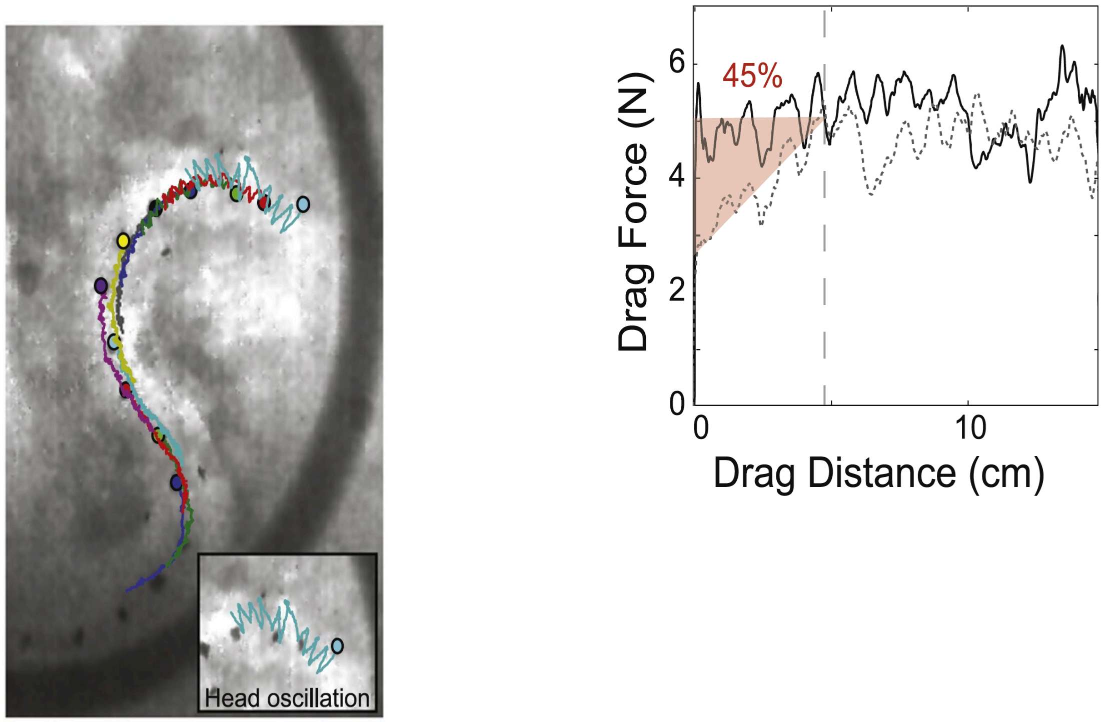

Figure 2: Left: X-ray picture of burrowing Ocellated Skink in damp sand. Head oscillation are tracked by colored lines. From Sharpe et al 2015, figure 7. Right: Drag forces experienced by a cylindrical intruder moving through damp granular media. The bold line represents the forces experienced without prior rotation, the dashed line represents the forces experienced following a single horizontal rotation of 20º from the centerline in both directions. From Sharpe et al 2015, figure 9

lowered the drag force experienced by a cylindrical intruder (3.81cm in length) by 45%, although this advantage was transient and disappeared after about 4cm (Fig. 2).

This thesis will address the knowledge gaps in our understanding of how kinematic strategies impact the forces involved with burrowing for squamates, particularly in damp granular media. It will also investigate the comparability of data obtained from burrowing simulations in damp sand and damp perlite. Specifically, the topics of investigation will include (1) the effect of varied oscillation ratio and amplitude on the forces required for burrowing, (2) the comparability of crushed perlite and sand as testing substrates for burrowing experiments, and (3) the effect of intermittency as opposed to simultaneous push and rotation (that is, whether the animal is rotating the head while pushing forward or stopping its forward push to rotate the head before continuing the forward movement).

My research will focus on a robophysical model – a mechanical device that simulates the geometry and kinematics of the organism of interest (Aydin et al., 2019; Aguilar et al., 2016). As mentioned earlier, the distinct morphologies and simple kinematics of amphisbaenians make them a suitable candidate for robophysical modelling. The model has further advantages over using live organisms due to the elusive nature amphisbaenians, and the scarcity of finding them alive in captivity (Hawkins et al., 2022). Additionally, robophysical models are programmable, which is of enormous benefit when studying locomotion underground in an environment that cannot be easily observed visually. In this way, we can control the movements of the test subject and be sure that it is performing these movements even when it cannot be seen. Further, using a robophysical model allows for the elimination of variables so that the experiment can focus only on the factors of interest and observe only specific behaviors (Koehl, 2003). Finally, with a robophysical model, we can directly measure the forces involved in locomotion, which is not typically possible in live animals.

Addressing the relationship between kinematics and penetration forces will help to provide data that can potentially be applicable for bioinspired engineering applications as described earlier, as well as for gaining insight into the evolution of limbless squamates. Comparison of sand and perlite will be useful in two ways. First, it will indicate the useability of perlite for similar laboratory work in the future. This could save much time, energy, and resources, potentially reducing the logistical burden of studying damp granular media. Second, since burrowing substrates vary widely in natural settings (Bergmann et al., 2017), it will be useful to gain insight as to the applicability of results across differing substrates.

CHAPTER II

METHODS

Robophysical Model

The central device used for my thesis is a robophysical testing apparatus, which mimics a simplified body plan of limbless, burrowing squamates. The specific application here is the investigation of patterns of movement in amphisbaenians. The robot can generate two independent movements: pushing forward through the substrate and moving the head laterally (Figure 3). Both shaft and head are actuated by hydraulic pistons. A hydraulic system, as opposed to a pneumatic one, is essential in this case so that the position of the submerged penetrator can be known although it is not visible. The hydraulic fluid, being incompressible, theoretically allows for a direct 1:1 transfer of motion from the piston to the robot. While this is theoretically the case, compliance in the walls of the tubing, and within the 3D printed components reduce the accuracy under high loads. While a small amount of compliance is less of an issue for the shaft, it needs to be accounted for in the head design because slight differences in the motion transfer can lead to significant differences in the expected head angle, and multiple changes of direction multiply any lag in the pressurization of the system. Therefore, a potentiometer was placed in the head, such that the cylindrical knob of the potentiometer acts as the axis of the rotating head. A cavity in the base of the head allows for a tight press-fit over the knob, but superglue was added to ensure adherence. As the head rotated, the potentiometer rotated, causing changes to a voltage reading in a separate circuit. Before trials, head angles were correlated to voltage readings, which were entered into the code controlling the head system. In this way, the robot was able to track the position of the head and so move to the desired amplitudes when instructed. The size of the hydraulic pistons places a lower limit on the size of the robophysical model, which is constructed of a 3D printed cylindrical shaft with a diameter of 5cm, and a bullet-shaped, moveable head 5cm in diameter at the base and tapering to a point at a distance of 7cm (see figure 3).

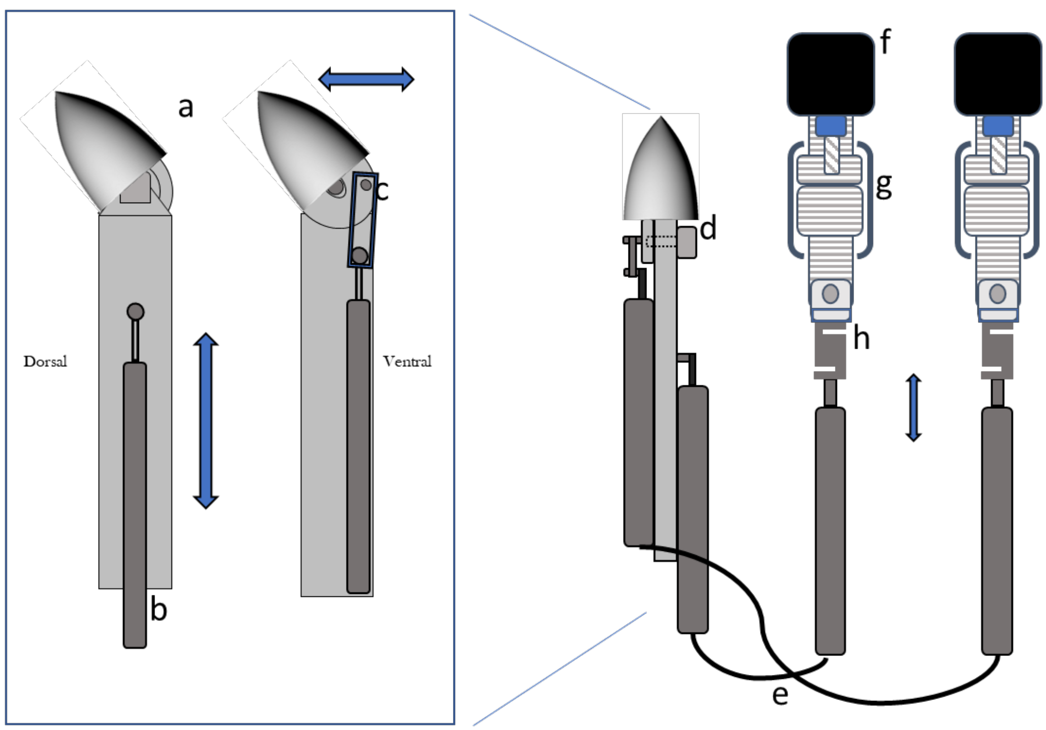

Figure 3: Schematic of testing apparatus. (a) 3D printed PLA head, (b) hydraulic piston, (c) slider crank linkage, (d) potentiometer, (e) hydraulic tubing, (f) stepper motor, (g) gear train, (h) load cell

One piston extends and retracts the shaft while a second, separate piston rotates the head through a slider-crank mechanism (see figure 3). These are connected through hydraulic tubing to two driving pistons, each coupled to a stepper motor by a 3D printed load cell. Thus the system is constructed with two separate sets of pistons – one driving the head and the other extending the shaft – each with a separate load cell monitoring the forces involved with the head and shaft separately. Throughout this thesis, “head force” will be used in reference to the forces involved with pushing the driving piston of the head, and “shaft force” will refer to those forces involved with driving the piston shaft. The stepper motors allow precise control of motion at high resolution across multiple cycles of rotation. A gear train amplifies the force output from the motors. Deformations in the load cells are sensed by two 350-ohm strain gauges connected in a half-Wheatstone bridge configuration to a custom amplifier (Gamel et al., 2024). Voltage output is recorded using a NIDAQ system and MATLAB to record the changes in load cell deformation caused by the force acting upon the driving pistons. Because the load cell is positioned immediately between the piston and the gear train, the recorded force will be identical to that applied via the piston to the substrate (after subtracting baseline data that record the force necessary to actuate the pistons). Calibration allows for these voltage outputs to be converted to force in Newtons; details of the calibration process are given in a subsequent section.

The stepper motors are controlled through an Arduino system. A limitation of the Arduino system is that only one stepper motor may be run at a time, making simultaneous head movement and shaft extension difficult. I addressed the problem by using two separate Arduino Uno boards, each running a separate program. One board contains the code to extend the shaft, specifying the distance and speed of the driving piston. Another board contains the code that controls the head. This code specifies the actions of the head driving piston. Feedback from the potentiometer in the head allows for the robot to move its head to the desired position, while the variables of amplitude, number of oscillations, and speed of oscillation can be specified ahead of time. The "Head" board sends a signal to the "Shaft" board when the shaft is to be activated (as determined by the defined kinematic strategy), allowing both motors to be operated simultaneously if desired, since each individual board is operating only one motor at once.

Substrate Preparation and Deposition

Following a simplified version of a method used by (Sharpe et al., 2015), we built a system for homogeneous deposition of damp granular media involving a metal mesh screen placed above the testing arena. Mesh sizes were 6.35mm for the sand trials, and 12.7mm for the perlite trials. Damp media in a separate tub was hoisted above the screen via a block and tackle system, and then sifted through the mesh. A similar "soil raining" deposition was found by the Goldman lab to produce a more even and homogeneous distribution of sand – avoiding the formation of voids in the testing area that could interfere with repeatable results (Sharpe et al., 2015). Repeated trials of the robotic penetrator verified that the mechanical properties of the material deposited in this way are indeed comparable among replicate trials (see figure 4).

The substrate was deposited into a 65x40cm tub, until the container was filled to a depth of 15cm (as indicated by a marking made on the inside of the tub ahead of time). At this point the robot was attached to a fixture mounted to the side wall. More of the substrate was then deposited to fill the tub to a depth of 30cm, leaving the tip of the robot submerged at the midpoint of the container and thus minimizing edge effects. This is important, as the jamming of granular media closer to walls can otherwise interfere with the forces that we want to record (Bergmann & Berry, 2021; Stone et al., 2004). Since the model is connected to the driving pistons through hydraulic tubing, the robot penetrator can be anchored to one end of the testing area and driven horizontally into the substrate. This eliminates depth effects – otherwise penetration into granular media is subject to a pressure that increases proportionally with depth, similar to the hydrostatic pressure experienced in fluids (Winter et al., 2014; Zhang & Goldman, 2014).

Force Data Collection and Analysis

The force required to operate the system when not submerged was recorded to use as a baseline (red lines in figure 4). Initially, the baseline trials were averaged and subtracted from the recorded forces during data analysis (green line) to provide visual representations of the force traces resulting entirely from submergence in wet sand (blue line). However, it is evident in figure 4 that the force increase while submerged in sand takes a longer period of time than that of the device when not submerged. The reason for this is unclear, but it has been consistently observed throughout the trials. The result is that when the baseline is subtracted, there is a transient period of negative force in the data. This does not affect the overall data analysis but makes the graphs difficult to interpret if the baseline is subtracted. Likewise, any offsets in the timing of head movements between the baseline and substrate datasets would lead to errors in the final variables. Thus, for clarity, the remainder of the images in my thesis will focus only on

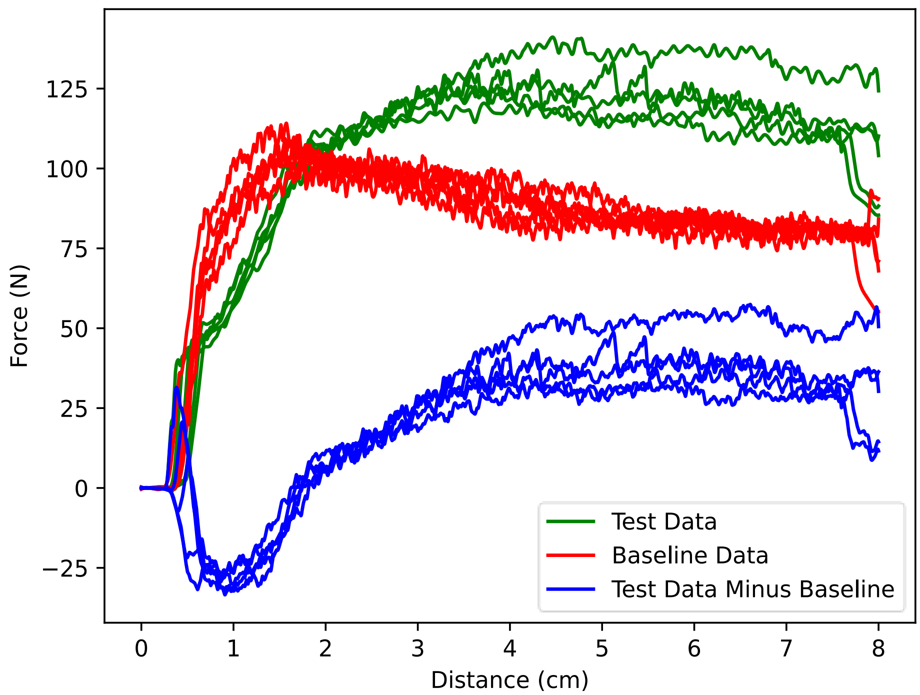

Figure 4: Preliminary data for multiple replicates. The red baselines indicate the force required just to overcome the friction of the machine and drive the intruder. The green lines indicate the force involved with movement through damp sand, and the blue lines show the total force minus the baseline – the force involved with the penetration alone.

the final variables, though figure 4 is useful as a representation of what is going on during the testing process. One factor to note is the relatively large deviations between replicate trials, which is more evident when the robot is submerged in sand and reflects the difficulty of preparing homogeneous batches of testing material. Further details concerning substrate and baseline analysis are discussed below.

The overall forces required for the robot to penetrate the substrate, in this case, involve two main components. First, there is the force involved with pushing the penetrator forward into the substrate. Second, there is the force involved with moving the head, should a head movement strategy be employed. The forces involved with the head movement create a potential tradeoff between the increase in rotational force and any reduction in penetration force that may result.

The robophysical model reconstructs a simplified body plan of a limbless burrowing squamate, allowing for programmed head motion and forward penetration that mimics those of amphisbaenians (as described in Gans 1968). The head excursion angle can be adjusted, and the number of head rotation cycles per total shaft extension (referred to here as oscillation ratio) can be changed through alterations in the Arduino coding to make the oscillation amplitude larger or smaller or to increase or decrease the number of sweeping motions in the case of oscillation ratio. The timing of the motor operation can likewise be changed in the coding, so that the head rotation can be coupled or decoupled from the forward penetration to look at the effects of intermittency. Although not investigated here, other factors such as head shape or direction of head motion could be easily adjusted by reconfiguring the head or rotating the position of the robot in future. The head is detachable from both the slider crank and the body, so that it could be swapped for other heads of differing configurations if desired.

Before running the trials, I calibrated the amplitude of the head movements using a protractor clamped into place just over the head of the robot, and a temporary line was marked on the tip of the head so that the angle of the sweep could be followed while the robot was operating. The voltage readings from the potentiometer circuit were noted for the desired angles, and incorporated into the coding as the robot's target settings.

Each set of trials involved the same basic steps. With the pistons detached from the driving apparatus and load cell, a multimeter was used to ensure that the Wheatstone bridge was balanced before the beginning of the trial, minor adjustments to the resistance being made using a built-in potentiometer in the circuit. The substrate was deposited through the shaker screen until the test arena was filled halfway, the halfway point having been previously measured with a meter stick and marked on the inside of the tub. At this point, the robot was attached to the mounting, and the substrate was deposited to reach the final depth. At the beginning of the trial, the tip of the robot was therefore positioned at an equal distance of 15cm from the top and bottom and an equal distance of 20cm from each side. Considering the mounting for the robot on the wall of the tub, the tip of the robot was at a starting position 23 cm from the end of the test arena, and an end position of 15 cm from the end of the test arena.

Before the machine was started, I began recording the data input from the NIDAQ through a custom MATLAB program. The machine was then engaged with the predetermined testing parameters, recording both head force and shaft forces simultaneously. Following each trial, a 25mL sample of the substrate was taken for thermo-gravimetric analysis of water content, to monitor for potential changes in moisture content over time (see Susha Lekshmi et al., 2014). The sample was placed in an oven and dried for 16 hours at 110°C, and then re-weighed to allow for calculation of the percent moisture content of the substrate at the time of the sampling. Moisture content was calculated as the dry weight of the substrate subtracted from the wet weight of the substrate. This was divided by the wet weight and multiplied by 100 to calculate the percent moisture content.

Since there was no need to synchronize simultaneous movements of the head and the shaft during the intermittent penetration trials, the parameters of amplitude, number of head rotations between forward pushes, and the distance of shaft movement for each push could simply be given to the robot at the beginning of each test. The coordination of the simultaneous head/shaft movements was slightly more complicated, as the speed of both stepper motors had to be adjusted in relation to one another so that the oscillation ratio was correct. Generally, the speed of the shaft's driving motor was kept constant, and that of the head's driving motor was increased or decreased so that it would complete its rotations at the same moment that the shaft completed its push.

Calibration of the load cells was done by vertically orienting and attaching them to a metal frame, so that weights could be suspended below them. In the case of the shaft load cell, a screw was set into the top of the load cell and a cord attached to the weights was looped around this, so that the hanging weights would compress the cell. Since the load cell on the head's driving piston was recording forces in both compression and tension, a similar process was used but with the addition of a step in which the load cell was inverted so that the weights were stretching rather than compressing the cell. Voltage readings were taken as an average of 3000 data points recorded by NIDAQ for each weight. As each weight experiences gravity, the force in Newtons can be calculated as $9.81 m/s^2$ times the weight in kg. The voltage readings increased linearly in relation to the force, so that the slope and the intercept of the linear increase could be calculated and used to convert experimental voltage data into force. This conversion was done in the custom Python program for both the shaft and the head. As the load cells were damaged now and then (especially during sand trials when high forces could cause them to snap), multiple calibration equations were involved, and thus a calibration table was created so that the appropriate conversion factor could be selected based on the date of the trial. A slightly different matrix needed to be developed for the head data, because the relationship between force and voltage, while still linear, was different in tension than in compression. The head calibration matrix therefore included different slopes and intercepts for tension and compression. An interactive data plot was developed, so that I could manually select the sections of the head force curve that corresponded to head movement. The code then automatically selected the appropriate conversion factor based on the section of movement.

Substrate Characterization

Before changing the testing substrate from sand to perlite, tests were performed to compare basic characteristics of each. The first test was to determine the avalanche angle of each substrate at varying moisture contents, so that a moisture content for perlite could be selected that matched the mechanics of the sand used for the sand trials. As mentioned above, the moisture content for the trials was monitored throughout the tests. When compared, the moisture content of the substrate for the penetration trials done in sand had a moisture content of 3.06% ± 0.41 by weight, and so the avalanche angle at this moisture level for sand was first determined and then used as the target avalanche angle for the perlite that would be used for the penetration trials in that substrate. The avalanche angle was determined through the tilting method (see Kalman, 2021). In this method, a small box measuring 27cm x 28cm constructed from polystyrene foam board (insulation board from Owens Corning) was filled to a depth of 1cm with the substrate. One end of the box was slowly lifted with a lifting platform from Precision Scientific Co., while the other end remained in place, until the substrate avalanched. This was filmed using a GoPro camera, so that images taken from the video could be analyzed using ImageJ image analysis software to measure the angle at which the avalanche began. The test was performed three times for each moisture content, and an average of the three angles was used as the avalanche angle for that moisture level. Dry substrate was hand-mixed with water separately before being transferred to the testing box. Standard deviations were high for the damp media, but a moisture content of 70% by weight for perlite approximately corresponded to the target avalanche angle, so this amount of water was used for the perlite trials that followed.

Additionally, the grain sizes of both dry sand and dry perlite were characterized using nested geological sieves. The particles captured by each progressive mesh size were weighed and recorded. This allowed for a distribution of grain sizes to be plotted and compared visually between both sand and perlite. Perlite was rinsed before the penetration trials, as the miniscule dust-sized grains seemed to contribute little to the size distribution, were easily airborne and caused respiratory irritation, and have been thought to lead to long-term health issues (although this is debated; see Roubik et al., 2022).

Variables and Data Processing

For the first set of experiments, comparing the results of the continuous push/head movement strategy between sand and perlite, the independent variables included substrate, oscillation ratio, and amplitude of head oscillation (the maximum angle of deviation from the centerline for each oscillation). The substrates included damp sand and damp perlite. Oscillation ratios tested were 1 and 2 rotations per 8cm penetration, at an amplitude of 15 degrees. Amplitudes of head oscillation included 5, 10, and 15 degrees at an oscillation ratio of 2. The dependent variables included peak force, average force, and total work involved for both the head and the shaft. The second set of experiments were conducted entirely in perlite as a testing substrate. Here, I again compared the amplitudes of 5, 10, and 15 degrees over oscillation ratios of 1 and 2 and against a control involving no head movement. Again, the dependent variables included peak force, average force, and total work. For the intermittent push strategies (the third set of experiments), the independent variables included the distance moved between head oscillations, oscillation ratio, and amplitude of head oscillation. The dependent variables included peak force, average force, and total work involved for both the head and the shaft.

Data processing was done using custom programs in Python. For all data, the raw voltage was splined before processing, and then converted into force in Newtons using the conversion factor as described above. From this, maximum forces, mean forces, and total work for each push were calculated. Peak forces and average forces were determined calculating maximum and averages from each dataset. Total work was computed using the numpy.trapz function in Python to integrate force with respect to distance in the case of the shaft, and to integrate force with respect to angular displacement (in radians) for the head.

For the intermittent trials, data processing was done in sections corresponding to the individual periods of motion for the shaft and the head. Maximum forces were reported as the maximum of forces compared across all sections. Average force was likewise an average of the forces for all sections. Work was calculated for each section, and the sum of these is reported.

Statistics

Statistics were done using JMP Pro 17 software. The large forces involved with penetration through damp sand limited the ability of the machine to complete enough trials for all parameters to be examined statistically using a 3-way ANOVA. For those trials involving sand, a 2-way ANOVA was done for the variables of oscillation ratio and substrate at an amplitude of 15 degrees, with fixed factors of oscillation ratio and substrate (sand or perlite) in a fully crossed design. Another 2-way ANOVA was done for the variables of amplitude and substrate at an oscillation ratio of 2, with fixed factors of amplitude and substrate in a fully crossed design. For continuous shaft motion trials through only perlite and including a head movement strategy, a 2-way ANOVA was done for the variables of oscillation ratio and amplitude, with fixed factors of oscillation ratio and amplitude in a fully crossed design. The same variables were compared between these trials and a control set involving no head movement, by using Tukey's HSD. ANOVAs could not be performed for controls, because having a value of zero for amplitude, oscillation ratio/number, and distance between oscillations lead to missing degrees of freedom that prevented the completion of analysis. For intermittent shaft motion trials, a 3-way ANOVA was done to compare each variable with fixed factors of oscillation number, amplitude, and distance between head oscillation phases in a fully crossed design. Due to the limited number of variables, Bonferroni correction was not applied, and the threshold for significance remained $p<0.05$ for both the overall model and effects. Differences between conditions within an effect which was significant were assessed using Tukey's Honest Significant Difference

CHAPTER III

COMPARISON OF SAND AND CRUSHED PERLITE AS A MEDIUM FOR BURROWING EXPERIMENTS

Introduction

Burrowing is by nature a process that involves high forces, which has been a large selective pressure in the evolution of burrowing animals (Evans et al., 2023; Herrel et al., 2021; Kazi & Hipsley, 2018; Wu et al., 2015). Among fossorial animals, this appears to have favored traits such as elongation, limblessness, a robust skull, and a narrow body plan (Gans, 1968; Bergmann et al., 2020; Deufel, 2017; Morinaga & Bergmann, 2020; Sharpe et al. 2014). Differing substrate characteristics such as grain particle shape and size influence the mechanics of the media, and thus the experience of the organism burrowing through it (Bergmann et al., 2017; Bergmann & Berry, 2021; Cho et al., 2006). Exactly how these differences play out in terms of animal locomotion is uncertain (Bergmann & Berry 2021). Nonetheless, substitutes for naturally-occurring media are common in experiments involving subterranean locomotion, including materials such as poppy seeds (Li et al., 2009), glass beads (Richefeu et al., 2006; Winter et al., 2014), and gelatin (Dorgan et al., 2005). The question of comparability between these various granular media analogues, mirroring the question of comparability between naturally-occurring substrates, is a topic of this chapter.

One of the major barriers to experimental work involving burrowing through naturally-occurring damp granular media has been the logistical difficulty involved with preparing repeatable batches of cohesive media for replicate trials (Sharpe et al. 2015). The work done for my thesis has confirmed that preparing these batches can be very time consuming (about 30-40 minutes per trial, assuming no failures occur). However, a greater challenge was related to the damage caused to the machine itself over time by performing repeated high-force trials through damp sand. At the beginning of my research, damp sand was the intended medium for all burrowing experiments, as it closely replicates natural environments while lacking organic components which would decompose over time, complicating comparisons. As the repeated high-force movements of the machine lead to constant component failures that were time-consuming to repair - with a failure occurring on average approximately once for every 5 or 10 successful trials - it became evident that damp sand was not a practical substrate for gathering datasets within our desired time frame and material availability. Moreover, the constant need to replace failed components resulted in a decreasing confidence in the comparability of data gathered over time, as the entire system was being replaced piece-by-piece.

Perlite ore is a naturally-occurring, lightweight, porous volcanic mineral, and I learned through informal experimentation that the commercially available crushed and expanded version of perlite has similar qualitative characteristics to sand when water is added, becoming cohesive and history-dependent with an increase in moisture. While lightweight, it tends to be reasonably resistant to crushing, generally failing (during informal experimentation) when pinched. If perlite can be used as an acceptable substitute in testing, it would relieve some of the experimental difficulties and might allow more research on damp granular media to be done in the future. This chapter focuses on a comparison of the mechanics of head movements and penetration forces through damp sand and damp perlite, both to establish the feasibility of using perlite as a substitute for sand in laboratory experiments involving damp granular media, and to help understand how burrowing data might be compared for organisms inhabiting different substrates.

Methods

The perlite used for the following experiments had a dry density of 0.06g/mL, compared to a density of 1.55g/mL for the dry sand. The sand used here was commercial play sand. Perlite and sand were characterized to compare avalanche angle (which is informative about the internal friction of the media) and particle size distribution. Before working with perlite, it was rinsed in water as an attempt to remove the fine dust particles that can cause respiratory irritation. Particle sizes were characterized for the perlite that had been used previously for robotic testing, and thus had been washed. Characterization took place following a period of drying at 110^{o}C for 16 hours. Both sand and perlite were sorted using nested geological sieves, and the weight of the particles contained in each size grade was weighed. The particle size distribution was characterized in terms of the coefficient of uniformity (C_u) and coefficient of curvature (C_c). These are dimensionless numbers that represent a ratio of the particle grain sizes present. Coefficient of uniformity is calculated as:

$$C_u = D_{60}/D_{10}$$

where D_{60} is the diameter of the particles at the point where 60% of the grains in the sample are of a smaller diameter, and D_{10} is the diameter of the particles at the point where 10% of the grains in the sample are of a smaller diameter. The coefficient of curvature is calculated as:

$$C_c = (D_{30})^2/D_{60}*D_{10}$$

where D_{30} is the diameter of the particles at the point where 30% of the grains in the sample are of a smaller diameter. The coefficient of uniformity estimates the range of particle sizes, such that a higher number has a wider variety of particle sizes. The coefficient of curvature refers to the evenness of this distribution, with a higher number reflecting more particle sizes spread between the highest and the lowest particle sizes (Ameratunga et al., 2016).

It was predicted that the mechanics of penetration through damp perlite would be similar to the mechanics of penetration in damp sand, the main difference being that the decrease in density would result in a similar decrease in force and work for both the head and the shaft in perlite.

Results

Prior to using perlite in the experiments, I characterized the particle size distribution of both dry perlite and dry sand, and avalanche angles for both sand and perlite of varying water contents (see chapter 2). The results of these characterizations are shown in Tables 1 and 2, and Figure 4. Since the sand trials had been done in sand with a moisture content of 3%, I used the sand avalanche angle at this moisture level (62.8 +/- 0.7 degrees) as the target avalanche angle for the perlite. In other words, I systematically increased the moisture content of the perlite until its avalanche angle matched that of sand at 3%. The behavior of damp perlite became increasingly unpredictable at higher moisture contents, as reflected in the higher standard deviations in Tables 1 and 2 (a similar increase in unpredictability with moisture has been noted in other work characterizing the mechanics of damp granular media (Mitarai & Nori, 2006). Overall, the mechanics of perlite at a water content of 70% by weight proved to be the closest approximation to the mechanics of sand at 3% (the moisture content at which the sand trials took place). This appears to correspond with the maximum saturation level of perlite – beyond 70%, excess water would drain to the bottom of the container leaving the bulk of the perlite near the 70% moisture level. This effect could be another advantage of using perlite, since even moisture contents could be more easily prepared and excess water could be removed. The higher water percentage for the perlite in comparison to sand may be due to the porosity of the perlite, meaning that some of the water is trapped inside the individual grains in a way that would not occur for sand. This higher percentage by weight could also be due simply to the fact that perlite grains weigh much less than sand grains, and so the same amount of added water in perlite will represent a higher proportional weight.

The particle size distributions show some differences (see figure 5). While some of this is an offset in scale, soil grading characteristics in terms of uniformity coefficient (C_u) and coefficient of curvature (C_c), which represent the distribution of particle sizes, differed. For sand, C_u = 1.75 and C_c = 0.89. For perlite, C_u = 19.46 and C_c = 9.52.

Table 1: avalanche angles for sand. The moisture content of the sand used in the sand trials is in bold print.

% Water content by weight	Avalanche angle (N=3)
0	30.2 +/- 1.2
1.3	34.2 +/- 1.0
1.9	41.2 +/- 2.3
2.6	54.9 +/- 1.7
3.03	**62.8 +/- 0.7**

Table 2: avalanche angles for perlite. The moisture content of the sand used in the sand trials is in bold print.

% Water content by weight	Avalanche angle (N=3)
0	34.5 +/- 1.5
65	46.2 +/- 1.7
68.6	48.2 +/- 10.9
71.3	56.8 +/- 2.2

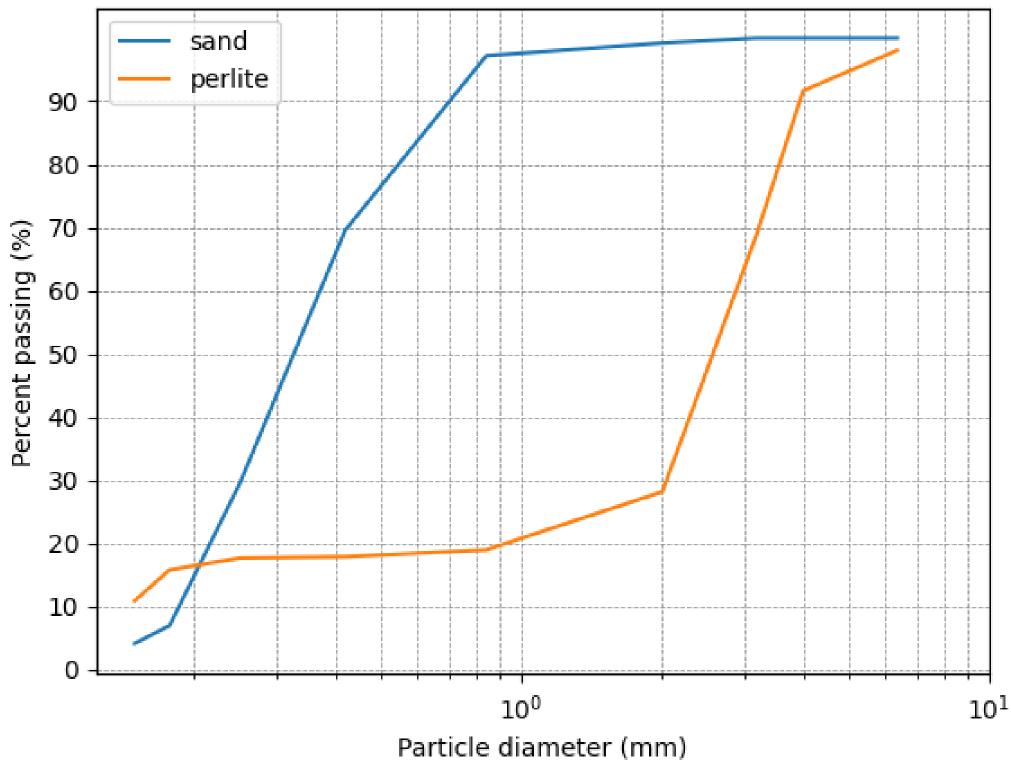

Figure 5: Grain size distribution of sand and perlite

As mentioned in chapter 2, the problems related to the high forces involved with penetrating through damp sand prevented the completion of sufficient replicate trials to conduct a 3-way ANOVA to compare all parameters (tables 3 and 4 show the number of replicate trials that were able to be conducted for each parameter, and thus gives an indication of the limitations of the system). Therefore, two 2-way ANOVAs were done in restricted sub-sets of the data which all contained at least 4 samples each, to do the following: (1) compare the variables of oscillation ratio and substrate (only for trials at an amplitude of 15 degrees), with fixed factors of oscillation ratio and substrate in a fully crossed design, and (2) compare amplitude and substrate (only for trials at an oscillation ratio of 2), with fixed factors of amplitude and substrate in a fully crossed design. The dependent variables were peak shaft penetration force, total work of shaft penetration, peak head force, average head force, and total head work. Because the shaft penetration distance is a constant throughout the trials, the results of the ANOVAs for average force and total work are identical, thus only peak shaft force and shaft work are reported. Because the lever arm is constant throughout the movements of the head, the head force will mirror torque, and therefore only head force will be referred to. Statistical results for the shaft data are summarized in tables 3 – 10, and the statistical results for the head data are summarized in tables 11 – 17.

Shaft results

Table 3: Number of successful trials for each parameter in sand

	Amplitude = 0	Amplitude = 5	Amplitude = 10	Amplitude = 15
Oscillation Ratio = 0	5	--	--	--
Oscillation Ratio = 1	--	1	1	5
Oscillation Ratio = 2	--	4	5	5

Table 4: Number of successful trials for each parameter in perlite

	Amplitude = 0	Amplitude = 5	Amplitude = 10	Amplitude = 15
Oscillation Ratio = 0	5	--	--	--
Oscillation Ratio = 1	--	5	5	5
Oscillation Ratio = 2	--	5	5	5

Table 5: One-way ANOVA comparing peak shaft force and total shaft work between sand and perlite for control groups

	F	**dF**	**P**
Peak force	0.65	1,8	0.44
Total work	0.72	1,8	0.42

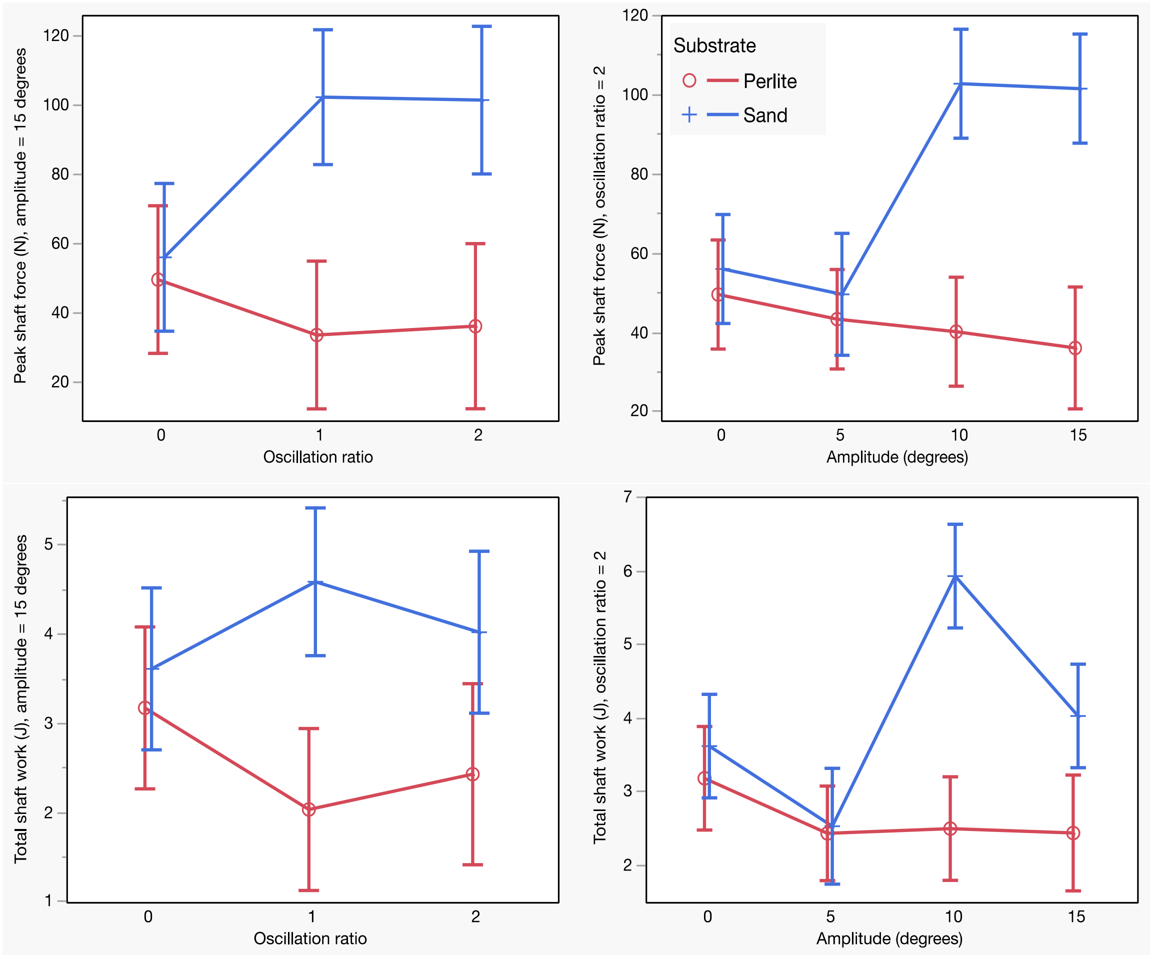

Figure 6: Peak shaft force and total shaft work for 15-degree amplitude oscillations at an oscillation ratio of 1 and 2 (left) and 5,10, and 15-degree amplitude oscillations at an oscillation ratio of 2 (right). Error bars represent the 95% confidence interval.

Table 6: Results of ANOVAs for shaft force and work

	F	dF	P
Peak shaft force (amplitude = 15 degrees)			
Whole model	10.34	3,16	**0.0005**
Substrate	30.49	**1,16**	**< 0.0001**
Oscillation ratio	0.0048	1,16	0.9458
Substrate x Oscillation Ratio	0.0197	1,16	0.8901
Peak shaft force (oscillation ratio = 2)			
Whole model	19.03	5,23	**<0.0001**
Substrate	56.77	**1,23**	**< 0.0001**
Amplitude	7.22	**2,23**	**0.0037**
Substrate x Amplitude	10.56	**2,23**	**0.0006**
Total shaft work (amplitude = 15 degrees)			
Whole model	6.99	**3,16**	**0.0032**
Substrate	18.80	**1,16**	**0.0005**
Oscillation ratio	0.317	1,16	0.8609
Substrate x Oscillation Ratio	1.0125	1,16	0.3293
Total shaft work (oscillation ratio = 2)			
Whole model	17.60	**5,23**	**<0.0001**
Substrate	36.23	**1,23**	**<0.0001**
Amplitude	12.95	**2,23**	**0.0002**
Substrate x Amplitude	11.97	**2,23**	**0.0003**

Table 7: Connecting letters report, Tukey's HSD, peak shaft force at an amplitude of 15 degrees

Substrate	**Oscillation**			**Least Squares Mean**
Sand	1	A		102.23833
Sand	2	A		101.37000
Perlite	1		B	33.33800
Perlite	2		B	35.88750

Table 8: Connecting letters report, Tukey's HSD, peak shaft force at an oscillation ratio of 2

Substrate	Amplitude			Least Squares Mean
Sand	5		B	49.43750
Sand	10	A		102.59600
Sand	15	A		101.37000
Perlite	5		B	43.15500
Perlite	10		B	40.00400
Perlite	15		B	35.88750

Table 9: Connecting letters report, shaft work at an amplitude of 15 degrees

Substrate	Oscillation				Least Squares Mean
Sand	1	A			4.5803333
Sand	2	A	B		4.0140000
Perlite	1			C	2.0260000
Perlite	2		B	C	2.4220000

Table 10: Connecting letters report, shaft work at an oscillation ratio of 2

Substrate	Amplitude				Least Squares Mean
Sand	5		B	C	2.5145000
Sand	10	A			5.9160000
Sand	15		B		4.0140000
Perlite	5			C	2.4170000
Perlite	10			C	2.4820000
Perlite	15			C	2.4220000

Peak shaft forces

The large error bars in the graphs in figure 6 may reflect the difficulty involved with consistent preparation of homogeneous batches of granular media (as mentioned in chapter 2). Nonetheless, at an amplitude of 15 degrees, the shaft experienced significantly higher forces in sand than in perlite ($p < 0.0001$). Despite the increase in peak force for sand, the error bars are large and the oscillation ratio did not have a significant impact on peak shaft penetration force at an amplitude of 15 degrees, nor was there a significant interaction effect.

At an oscillation ratio of 2, there was again a statistically significant relationship between substrate and peak shaft penetration force, with the peak shaft force being higher in sand than in perlite ($p < 0.0001$). There was also a significant relationship between amplitude and peak shaft penetration force ($p = 0.0037$), as well as a statistically significant interaction between substrate and amplitude on peak shaft penetration force ($p < 0.0006$). Overall, the mean of the peak shaft forces were significantly less at an amplitude of 5 degrees than at amplitudes of 10 and 15 degrees. However, this transition to higher force is only apparent in the sand trials. In the perlite there is a slight but not statistically significant decrease in peak forces with increasing amplitude.

Total shaft work

At an amplitude of 15 degrees, the work done by the penetrating shaft was again significantly higher in sand than in perlite ($p < 0.0005$). At an oscillation ratio of 2, this same relationship between substrates is evident ($p < 0.0001$). There was also a significant increase in shaft penetration work from an amplitude of 5 degrees to an amplitude of 10 degrees ($p = 0.0002$), followed by a significant increase in work with a continued increase in amplitude up to 15 degrees ($p = 0.0257$). There was a statistically significant interaction between substrate and amplitude on total shaft penetration work ($p = 0.0003$) and figure 6 shows that the significant changes in work are again evident in the sand trials but not in the perlite trials.

Head results

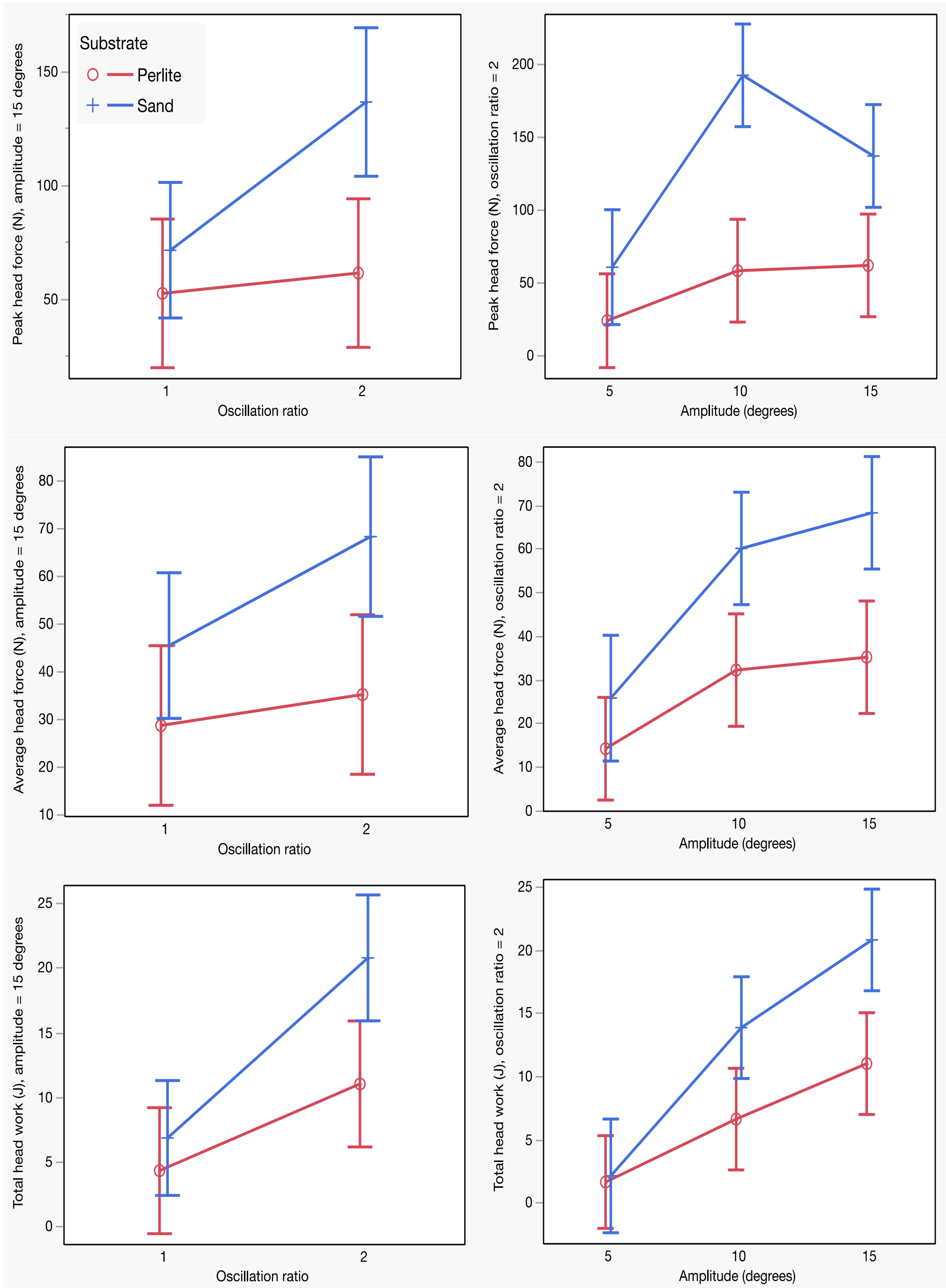

Figure 7: Peak head force, average head force, and total head work for 15-degree amplitude oscillations at an oscillation ratio of 1 and 2 (left) and 5,10, and 15-degree amplitude oscillations at an oscillation ratio of 2 (right). Error bars represent the 95% confidence interval.

Table 11: Results of 2-way ANOVAs for head forces and work

	F	dF	P
Peak head force (amplitude = 15 degrees)			
Whole model	8.75	3,16	0.0011
Substrate	8.861	**1,16**	**0.0089**
Oscillation ratio	14.537	**1,16**	**0.0015**
Interaction	2.009	1,16	0.1677
Peak head force (oscillation ratio = 2)			
Whole model	16.91	5,23	<0.0001
Substrate	34.575	**1,23**	**<0.0001**
Amplitude	16.156	**2,23**	**<0.0001**
Interaction	5.659	**2,23**	**0.0100**
Average head force (amplitude = 15 degrees)			
Whole model	8.24	**3,16**	**0.0015**
Substrate	11.102	**1,16**	**0.0042**
Oscillation ratio	12.946	**1,16**	**0.0024**
Interaction	0.159	1,16	0.6955
Average head work (oscillation ratio = 2)			
Whole model	27.43	5,23	<0.0001
Substrate	35.389	**1,23**	**<0.0001**
Amplitude	42.212	**2,23**	**<0.0001**
Interaction	1.986	2,23	0.1601
Total head work (amplitude – 15 degrees)			
Whole model	36.78	3,16	<0.0001
Substrate	10.546	**1,16**	**0.0050**
Oscillation ratio	94.769	**1,16**	**<0.0001**
Interaction	1.569	1,16	0.2283
Total head work (oscillation ratio = 2)			
Whole model	54.12	5,23	<0.0001
Substrate	26.053	**1,23**	**<0.0001**
Amplitude	108.668	**2,23**	**<0.0001**
Interaction	5.534	**2,23**	**0.0109**

Table 12: Connecting letters report from Tukey's HSD, peak head force at an amplitude of 15 degrees

Substrate	Oscillation			Least Squares Mean
Sand	1		B	71.27000
Sand	2	A		136.27000
Perlite	1		B	52.33600
Perlite	2		B	81.60500

Table 13: Connecting letters report from Tukey's HSD, peak head force at an oscillation ratio of 2

Substrate	Amplitude				Least Squares Mean
Sand	5			C	60.04700
Sand	10	A			191.54800
Sand	15	A	B		136.27000
Perlite	5			C	23.37500
Perlite	10			C	57.61200
Perlite	15		B	C	81.60500

Table 14: Connecting letters report from Tukey's HSD, average head force at an amplitude of 15 degrees

Substrate	Oscillation			Least Squares Mean
Sand	1		B	45.346389
Sand	2	A		68.156000
Perlite	1		B	28.604000
Perlite	2	A	B	46.865000

Table 15: Connecting letters report from Tukey's HSD, average head force at an oscillation ratio of 2

Substrate	Amplitude						Least Squares Mean
Sand	5				D	E	25.713700
Sand	10	A	B				59.990400
Sand	15	A					68.156000
Perlite	5					E	14.126667
Perlite	10			C	D		32.144000
Perlite	15		B	C			46.865000

Table 16: Connected letters report from Tukey's HSD, head work at an amplitude of 15 degrees

Substrate	Oscillation				Least Squares Mean
Sand	1			C	6.796667
Sand	2	A			20.758000
Perlite	1			C	4.262000
Perlite	2		B		15.040000

Table 17: Connected letters report from Tukey's HSD, head work at an oscillation ratio of 2

Substrate	Amplitude					Least Squares Mean
Sand	5			C	D	2.116000
Sand	10		B			13.828000
Sand	15	A				20.758000
Perlite	5				D	1.628333
Perlite	10			C		6.602000
Perlite	15		B			15.040000

Peak head forces

At an amplitude of 15 degrees, the peak head forces experienced in sand were significantly higher than those experienced in perlite ($p = 0.0089$). The peak head forces were higher at an oscillation ratio of 2 than at an oscillation ratio of 1 ($p = 0.0015$). At an oscillation ratio of 2, the peak head force was again significantly higher in sand than in perlite ($p < 0.0001$). There was also a significant increase in peak head force from an amplitude of 5 degrees to an amplitude of 10 degrees ($p < 0.0001$) and 15 degrees ($p = 0.0009$). There was again a statistically significant interaction between substrate and amplitude on peak head force ($F_{2,23} = 5.659$, $p = 0.0100$). Figure 7 shows that the significant changes in peak force are only seen in the sand trials, and not in the perlite trials.

Average head force

At an amplitude of 15 degrees, the average head force moving through perlite was significantly lower than the average head force of moving through sand ($p = 0.0042$). The average head force at an oscillation ratio of 1 was significantly lower than the head force at an oscillation ratio of 2 ($p = 0.0024$). At an oscillation ratio of 2, the average head force in perlite was significantly lower than the average head force in sand ($p < 0.0001$). The average head force increased significantly with amplitude from 5 to 10 degrees ($p < 0.0001$) and again from 10 to 15 degrees ($p=0.0304$).

Head work

At a constant amplitude of 15 degrees, the total head work was significantly less in perlite than in sand ($p < 0.0050$), and significantly less for trials involving an oscillation ratio of 1 compared to those with an oscillation ratio of 2 ($p < 0.0001$).

At an oscillation ratio of 2, the total head work was again less in perlite than in sand ($p < 0.0001$), and increased with increasing amplitude from 5 to 15 degrees with each pairwise difference being significant. There was a significant interaction between substrate and amplitude on total head work ($p = 0.0109$), with the head work increasing at a steeper angle with amplitude in the sand than in the perlite.

Discussion

Shaft peak force and work are not significantly different between sand and perlite in the control groups (see table 5), but significant differences arise when head oscillations are taking place. This suggests that the pressure from the overlying substrate is not the primary force opposing the motion of the robophysical model. Within substrates, overall trends showed some similarities with respect to the peak force and total work for the variables examined, more so for the head than for the shaft. For all parameters, there was a significant relationship between substrate and peak force, average force, and total work, these values being higher for sand than for perlite. This is expected, considering that the sand had a much higher density than perlite (0.06g/mL for dry perlite, compared to a density of 1.55g/mL for dry sand). The two factor graphs indicate that the response of the forces and work for the head are similar in both sand and perlite at an amplitude of 15 degrees. There is a significant interaction between substrate and amplitude in their effect on force and work for both shaft and head at an oscillation ratio of 2. The most obvious difference is the increase in peak force and work in sand for the shaft at an amplitude of 10 degrees and an oscillation ratio of 2 (see figure 6). For a head that is longer than it is wide, a larger rotation angle would present a larger surface area at the tip of the intruder, and thus could an increase in penetration force could make sense if the oscillation is not serving to decrease the penetration force in some other way (Liu et al., 2019). However, it is uncertain why there is such a sharp increase in force at an amplitude of 10 degrees in sand, while such a sharp increase is not seen in perlite. If sand and perlite mechanics are similar in effects but different in scale, it is possible that a similar trend in perlite might arise if higher amplitudes are examined.

However, it is possible that the mechanics differ between sand and perlite here. Individual amphisbaenians of the genus *Rhineura* have been observed to change penetration strategy based on the compaction of the soil through which they burrow (Gans, 1960). Head rotation has been observed to occur in more compacted soils, while it has been absent in looser soils (Gans, 1960). This observation has been cited in support of the idea that head rotation lowers the force and/or work of burrowing, suggesting that those individuals facing more compact soils are adopting the head rotations out of the need to decrease the penetration force (Gans, 1960). The results in this chapter suggest that the change in strategy could also be related to a shift in substrate behavior from lighter to denser soils, larger to smaller particle size, or both. For example, particle size has been found to be a determining factor in the force required for vertical penetration of granular media (Bergmann & Berry, 2021), and also a determining factor on the stability of tunnels (Shinoda et al., 2018). For the parameters examined here, changes in head rotation seemed to make little difference on shaft force and work in the less dense and substrate (perlite), while making a significant difference in the case of the denser sand. Although the difference here is an increase in force and work after an amplitude of 5 degrees, figure 6 indicates a sensitivity of total work to head rotation that is not necessarily linear.

While informal experimentation indicated that sand and perlite behave similarly, quantification of the characteristics of the sand and perlite used here indicate notable differences in terms of uniformity coefficient (C_u) and coefficient of curvature (C_c). Specifically, the sand was more uniformly graded than the washed perlite, while the perlite had a wider distribution of particle sizes. These differences in size distribution could be part of the reason for the differing mechanics. Selection of particle sizes might have allowed for a more comparable grading between the two substrates, but would have been both time consuming and potentially cost-prohibitive, and purchasing perlite means being limited to the commercially available size grades. For the purposes of this thesis, the grading differences were unavoidable.

Despite these differences and the differences between sand and perlite for peak penetration force and work at 2 head oscillations of 10 and 15 degrees, some aspects examined appear to be comparable. Avalanche angles are linear with respect to moisture content, though offset in scale. Peak forces, average forces, and total work show somewhat similar trends between sand and perlite for the head data, with some scaling differences. And the lack of significant difference between control groups in sand and perlite suggest a similarity in penetration resistance. Still, the results of this chapter suggest caution when generalizing results across substrates. Although it does not invalidate the use of perlite, there are possible implications for laboratory research involving substitutes for naturally occurring granular media, and for comparison of organisms moving through different substrates outside of the lab. More research may be needed to ascertain where important differences in mechanics arise, and how these differences affect the data obtained. Meanwhile, it raises some thought-provoking questions about burrowers in natural habitats. Burrowing organisms inhabit a wide range of materials from leaf litter to gravel (Bergmann & Morinaga, 2019, Bergmann & Berry 2021), and it is unlikely that these substrates are homogeneous within the geographic range of individuals. Therefore, not only are burrowing organisms potentially facing widely different mechanics depending on choice of habitat, they may also be facing changing mechanics and greater differences than might be assumed within seemingly similar media.

CHAPTER IV

THE EFFECT OF VARIED OSCILLATION RATIO AND AMPLITUDE ON THE FORCES REQUIRED FOR BURROWING

Introduction

In organisms such as amphisbaenians, side-to-side and vertical head movements may function to compact soil into the sides or the roof of a tunnel (Gans 1968; Gans 1978), or alternatively, the side-to-side movements could function to decrease the required force of an organism's penetration through granular media (Sharpe et al. 2015). Oscillatory movements have been associated with a decrease in penetration resistance experimentally (Sharpe et al., 2015; Tang et al., 2024; Tang & Tao, 2022, Del Dottore, 2018), and this decrease in resistance has been suggested to be a reason for circumnutation (i.e., oscillatory growth of root tips) in plants (Del Dottore, 2018). However, there is little published data quantifying the effects that head movements such as amplitude (excursion angle from a center point) and oscillation ratio (head oscillations per total shaft extension) have on penetration through wet media in terms of force and work. To my knowledge, there is only one published study directly quantifying this relationship. Sharpe et al. (2015) looked at the burrowing behavior of Ocellated Skinks, observing that they employed a side-to-side head movement at about 2-4 Hz while moving through both dry, non-cohesive sand, and wet, cohesive sand (Sharpe et al. 2015). The angle of head oscillation differed, reaching a maximum of 7.6 +/- 2.3 degrees in dry sand and 4.5 +/- 1.3 degrees in wet (Sharpe et al. 2015). They hypothesized that this behavior may function to decrease the required penetration force for the organism moving through granular media (Sharpe et al. 2015), though it could be simply the instinctual use of a behavior adapted for wet media in all situations. They then performed tests in which they submerged a cylindrical rod in both dry and damp sand, followed by a single rotation to an amplitude of 20 degrees, and then by a single push through the substrate. This resulted in a transient 45% decrease in yield force that disappeared after 4cm in wet sand, though little decrease in yield force was noted in dry sand (Sharpe et al. 2015).

To further explore the relationship between head oscillations and burrowing at different amplitudes and for a continuous head rotation coupled with forward penetration, I systematically varied the parameters of amplitude and oscillation ratio (that is, the number of oscillations per shaft extension) and recorded the force and total work for both the forward penetration of the shaft and the lateral rotation of the head of the robophysical model (described in chapter 2 of this thesis) in damp granular media. I hypothesized that, as in the Sharpe et al 2015 experiments, head motion would be associated with a reduction in penetration force, and that these effects would be greater at higher amplitudes and with more oscillations. Experiments were conducted using damp perlite as a proxy for naturally occurring damp granular media. Head oscillation ratios of 0, 1, and 2 oscillations per shaft extension were tested, at excursion angles of 0, 5, 10, and 15 degrees from centerline. Details of methods and analysis are found in Chapter 2.

Results

Statistical results for the shaft data are shown in tables 16 – 20, and those for the head data are shown in tables 21-24. Table 16 gives the results for the ANOVAs done for peak shaft force and total shaft work at amplitudes of 5, 10, and 15, and at oscillation ratios of 1 and 2. Because the results of the ANOVA for the shaft force and work at these parameters were insignificant, no post hoc tests were done. 2 and 3-way ANOVAs could not include the control because amplitudes and oscillation ratios of 0 lead to missing degrees of freedom. Instead, means were compared using Tukey's HSD. The connecting letters reports are shown in tables 18 – 22. Table 21 gives the results of the 2-way ANOVA for the head data, and tables 23-26 are the associated Tukey's HSD test connecting letters reports.

Shaft Results

Although the graphs show a slight decrease in peak force and total work, ANOVAs do not indicate any significant relationship either between amplitudes of 5, 10, and 15 degrees or an oscillation ratio of 1 or 2 on either peak shaft force or total shaft work (see table 18). Tukey's HSD also indicates no significant differences when the control groups (with no head movement) are included.

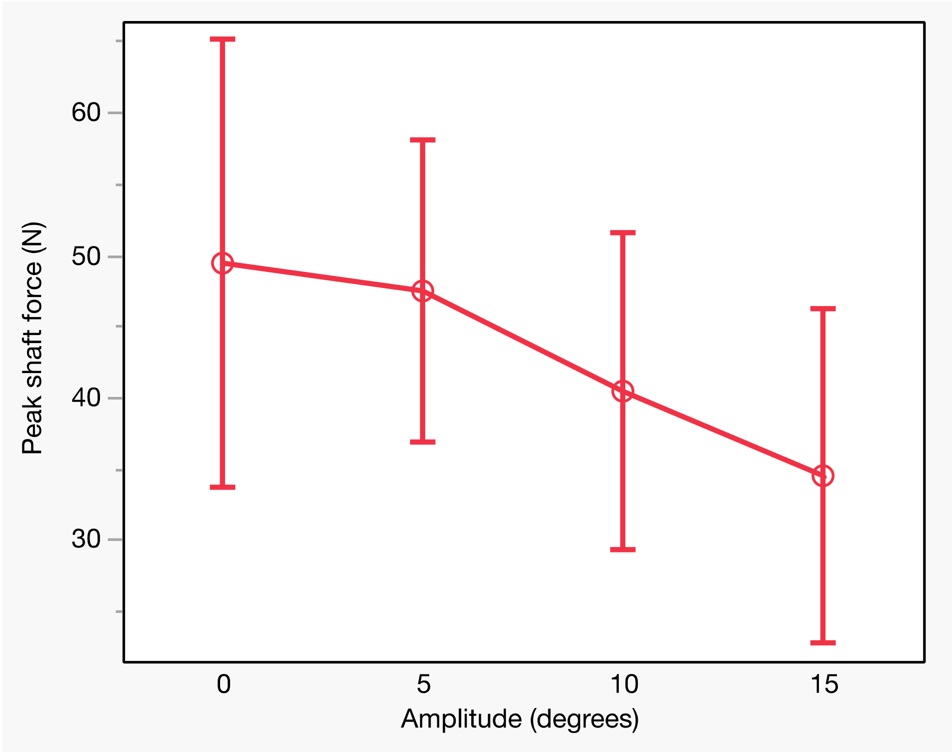

Figure 8: Peak shaft force vs amplitude of head movement. Error bars represent the 95% confidence interval.

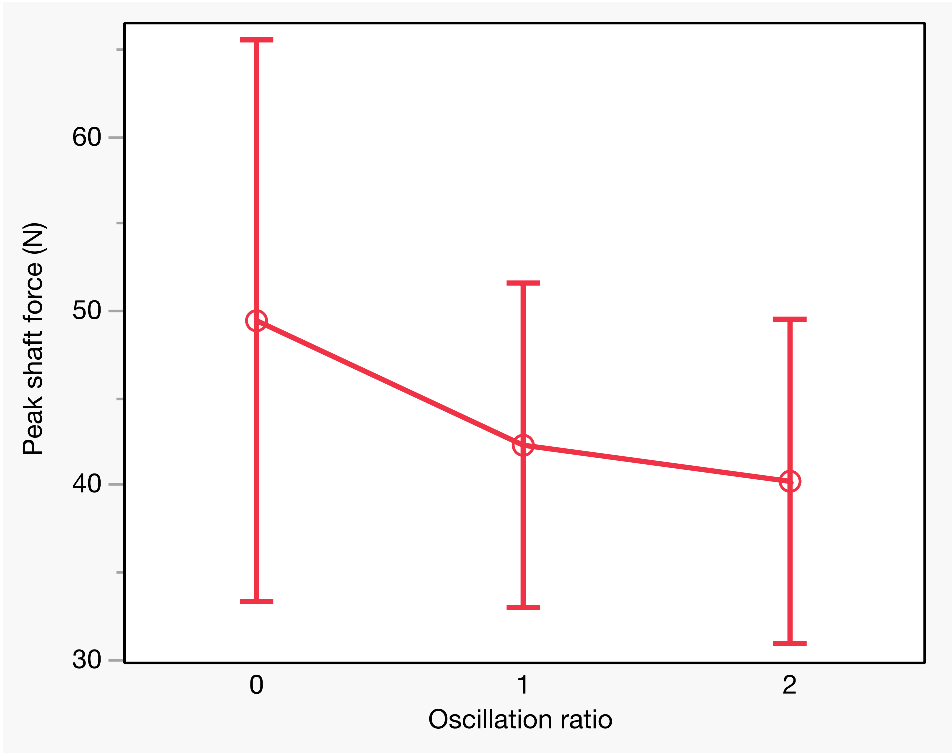

Figure 9: Peak shaft force vs oscillation ratio. Error bars represent the 95% confidence interval.

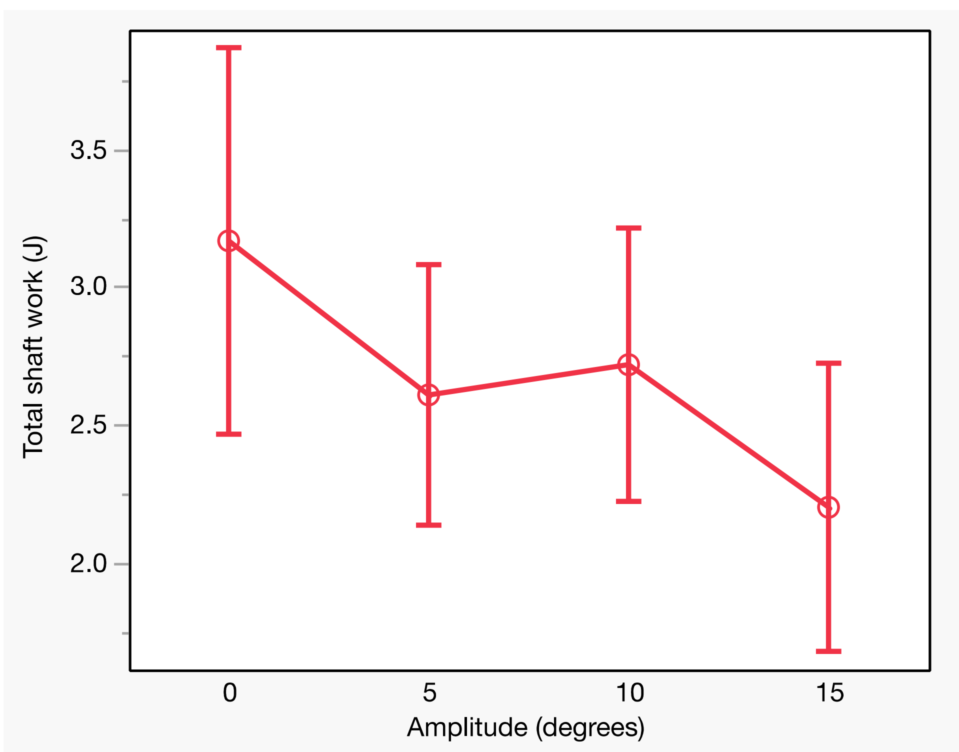

Figure 10: Total shaft work vs amplitude of head movement. Error bars represent the 95% confidence interval.

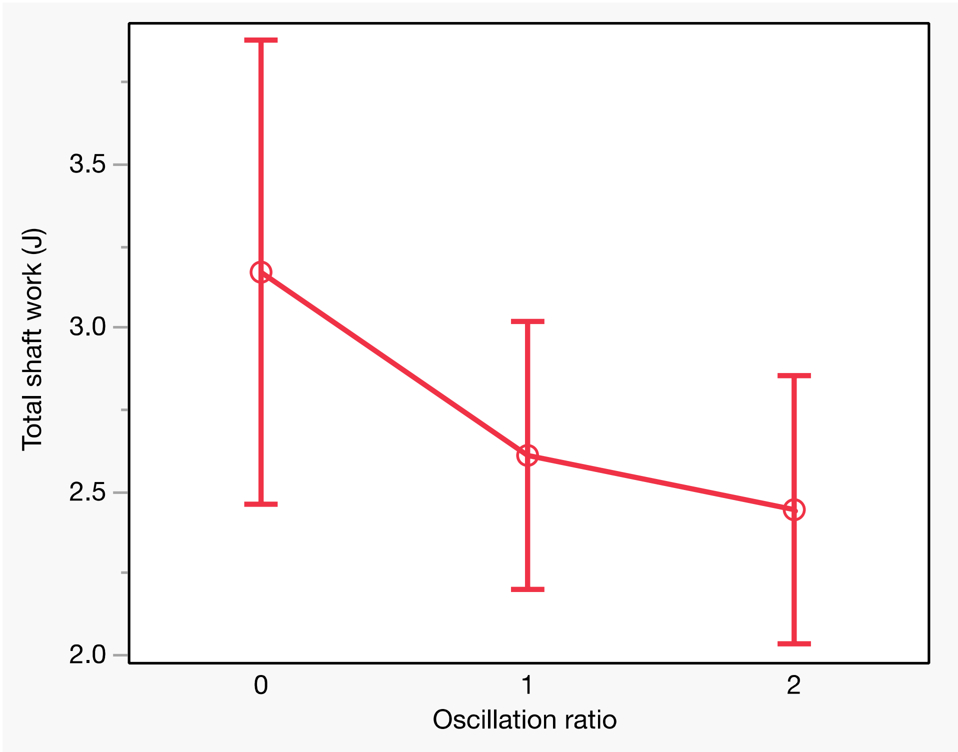

Figure 11: Total shaft work vs oscillation ratio. Error bars represent the 95% confidence interval.

Table 18: Results of a 2-way ANOVA comparing the peak shaft force and total shaft work of the robotic penetrator at amplitudes of 5, 10, and 15 degrees, and oscillation ratios of 1 and 2

	F	dF	P
Shaft Peak Force			
Whole model	0.61	5,24	0.69
Amplitude	1.22	2,24	0.31
Oscillation	0.13	1,24	0.72
Amplitude*Oscillation	0.27	2,24	0.77
Total shaft work			
Whole model	0.91	5,24	0.49
Amplitude	1.05	2,24	0.37
Oscillation	0.33	1,24	0.57
Amplitude*Oscillation	0.90	2,24	0.42

Table 19: Connecting letters report from Tukey's HSD for the peak shaft force of the robotic penetrator at amplitudes of 5, 10, and 15 degrees to a control group of no head movement

Amplitude		**Mean**
0	A	49.388000
5	A	47.436364
10	A	40.401000
15	A	34.471111

Table 20: Connecting letters report from Tukey's HSD for the total shaft work of the robotic penetrator at amplitudes of 5, 10, and 15 and a control group with no head movement

Level		**Mean**
0	A	3.1660000
5	A	2.6083636
10	A	2.7180000
15	A	2.2020000

Table 21: Connecting letters report from Tukey's HSD for the peak shaft force of the robotic penetrator at oscillation ratios of 1 and 2 and a control group with no head movement

Level		**Mean**
0	A	49.388000
1	A	42.236667
2	A	40.166667

Table 22: Connecting letters report from Tukey's HSD for the peak shaft force of the robotic penetrator at oscillation ratios of 1 and 2 to a control group with no head movement

Level		**Mean**
0	A	3.1660000
1	A	2.6060000
2	A	2.4400000

Head Results

There was a significant relationship between both amplitude and oscillation ratio on peak head force, average head force, and total head work (see table 23). Peak head force was significantly lower at an amplitude of 5 degrees than at amplitudes of 10 degrees ($p < 0.0001$) or 15 degrees ($p < 0.001$). Average increased with increasing amplitude, with each pairwise difference being significant. Similarly, the total work done by the head increased with increasing amplitude, with each pairwise difference being significant. Peak head force at an oscillation ratio of 1 was significantly lower than the peak head force at an oscillation ratio of 2 ($p < 0.0001$), as was the average head force ($p < 0.0001$), and the total head work ($p < 0.0001$).

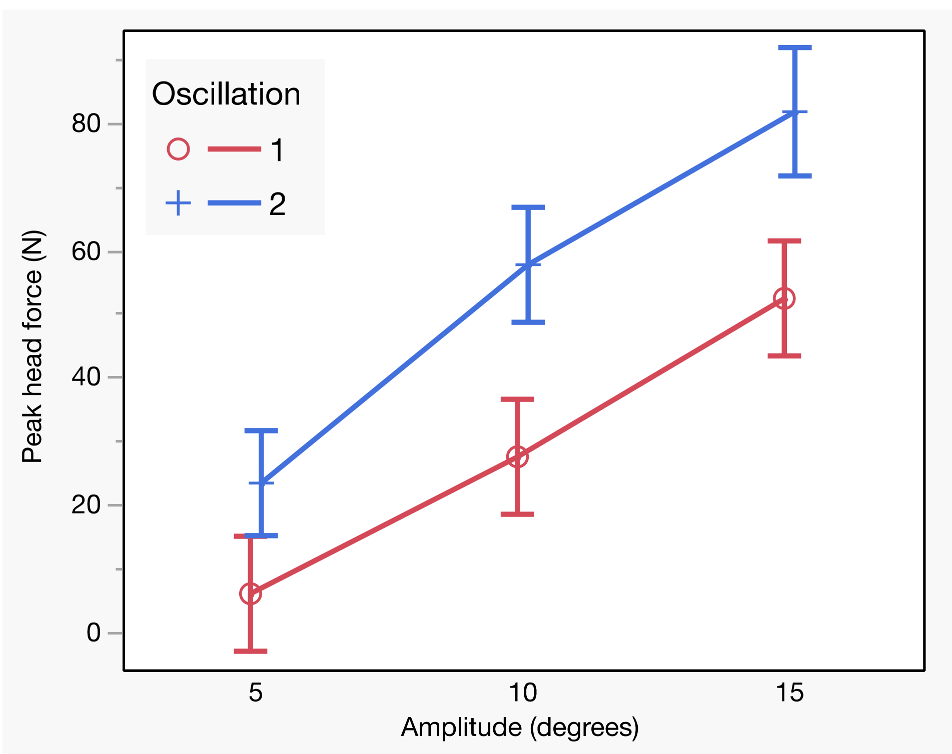

Figure 12: Peak head forces vs amplitude, at oscillation ratios of 1 and 2. Error bars represent the 95% confidence interval.

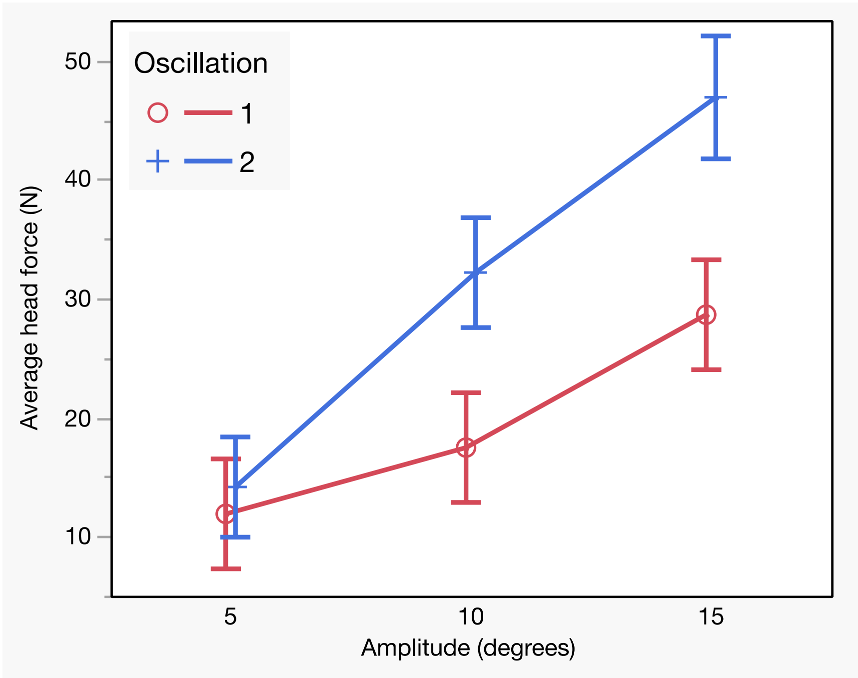

Figure 13: Average head force vs amplitude, at oscillation ratios of 1 and 2. Error bars represent the 95% confidence interval.

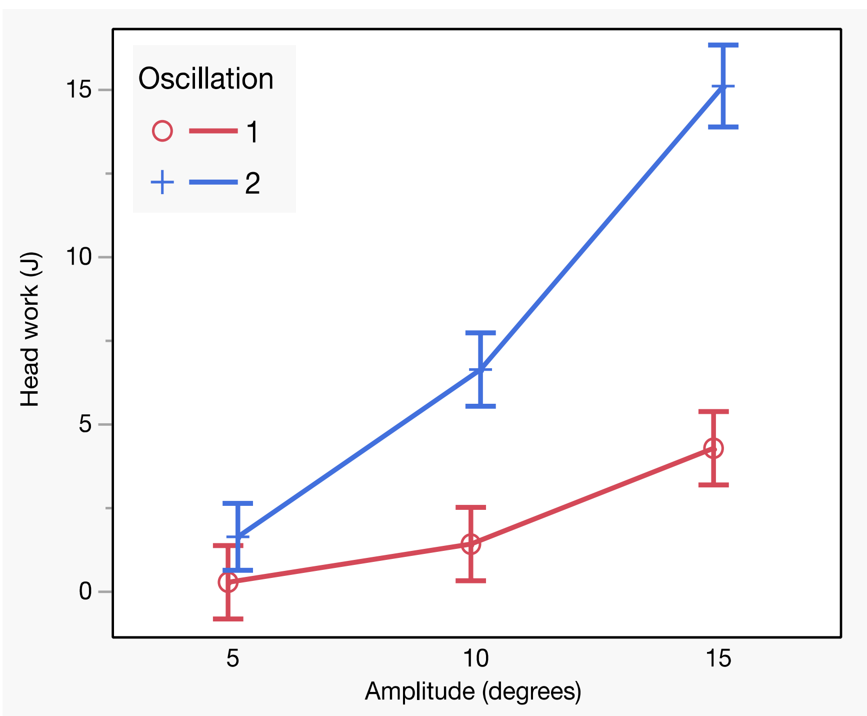

Figure 14: Total head work vs amplitude, at oscillation ratios of 1 and 2. Error bars represent the 95% confidence interval.

Table 23: Results of a 2-way ANOVA indicating the relationships between peak head force, average head force, and total head work of the robotic penetrator at amplitudes of 5, 10, and 15 degrees, and oscillation ratios of 1 and 2

	F	dF	P
Head peak force			
Whole model	36.60	5,24	< 0.0001
Amplitude	70.88	2,24	< 0.0001
Oscillation	50.76	1,24	< 0.0001
Amplitude*Oscillation	1.39	2,24	0.27
Head average force			
Whole model	32.53	5,24	< 0.0001
Amplitude	60.03	2,24	< 0.0001
Oscillation	40.80	1,24	< 0.0001
Amplitude*Oscillation	7.20	2,24	0.0036
Total head work			
Whole model	93.36	5,24	< 0 .0001
Amplitude	134.19	2,24	< 0.0001
Oscillation	176.29	1,24	< 0.0001
Amplitude*Oscillation	39.00	2,24	< 0.0001

Table 24: Connecting letters report from Tukey's HSD, peak head force

Amplitude	**Oscillation**					**Least Squares Mean**
15	2	A				81.605000
10	2		B			57.612000
15	1		B			52.336000
10	1			C		27.508000
5	2			C	D	23.375000
5	1				D	6.042000

Table 25: Connecting letters report from Tukey's HSD, average head force

Amplitude	**Oscillation**				**Least Squares Mean**
15	2	A			46.865000
10	2		B		32.144000
15	1		B		28.604000
10	1			C	17.440000
5	2			C	14.126667
5	1			C	11.870000

Table 26: Connecting letters report from Tukey's HSD, total head work

Amplitude	Oscillation					Least Squares Mean
15	2	A				15.040000
10	2		B			6.602000
15	1			C		4.262000
5	2				D	1.628333
10	1				D	1.410000
5	1				D	0.278000

Discussion

Rotational movements have been found to decrease penetration resistance in granular media (Tang et al., 2024; Tang & Tao, 2022). It is possible that the side-to-side head movements disrupt force chains (Xue et al., 2024), propagate "cracks" in cohesive soils (Sharpe et al., 2015). However, the results of this experiment suggest that any advantage in terms of reduced force or work might be offset by the significant increase in head forces involved. In this case, a head oscillation with a 15-degree amplitude decreased the mean peak force of the shaft by 14.92N, and the total work of the shaft by 0.97J. Meanwhile, the mean of the peak forces required to rotate the head at this angle is 65.34N, and the total work done by the head for one oscillation at this amplitude is 9.05J. If all forces and work are considered together for the head and the shaft, the requirement for moving the head outweighs the advantage, at least for this robot.

It is also possible that the behavior serves another purpose to which the decrease in penetration force and work is a byproduct. For example, Sharpe et al. (2015) hypothesized that head movements made by Ocellated Skinks (*Chalcides occelatus*) while burrowing could be a strategy to locate regions of looser compaction in granular media. In trials where replicate batches of sand lacked homogeneity, the animal would move in the direction of these lesser compacted areas (Sharpe et al. 2015). Ducey et al. (2003) observed through laboratory experiments that caecilians preferred looser soils, actively moving over the surface and prodding the soil with their heads before selecting a location for digging. Amphisbaenians appear to select habitats based on soil characteristics as well. Martín et al. (1991) observed that the amphisbaenian *Blanus cinereus* preferred soils with a lower clay content over those with a higher clay content, hypothesizing that the preference was related to the ease of digging. Martín et al. (2021) similarly observed that *Trogonophis wiegmanni* prefer looser to more compact soils.

Carl Gans noted that amphisbaenians burrowing in looser soils did not use the head rotation strategy, while they did use it in more compact soils (Gans 1960). This might suggest that differences in substrate mechanics make the head oscillation strategy less advantageous in some conditions and more advantageous in others. The experiments in this chapter looked at only one type and compaction of granular media, and advantages to head oscillation might only arise in more compact substrates.

Another possibility is that the head movements are meant primarily for tunnel construction by packing material and forming walls, and have little to do with the initial cost of penetration. Tunnel construction was the suggestion made by Gans (1968). Amphisbaenians reuse permanent tunnels which can serve multiple purposes. One of these is the volumetric expansion of the organism that occurs during respiration, and thus requires at least a minimum tunnel diameter (Gans 1968). Also, of course, a permanent tunnel can be used repeatedly regardless of the initial cost, thus force and work would be greatly reduced for subsequent uses.

Another important factor to consider in this experiment is that the head shape of the robot was not biologically inspired. The force required to push through a substrate is dependent on head shape (Bergmann & Berry, 2021; Mishra et al., 2018), and linearly proportional to the cross-sectional area of the intruder (Liu et al., 2019). Therefore the force that the head would need to generate for lateral rotations into the substrate would be sensitive to the geometry of the head. Indeed, head shapes appear to be correlated with burrowing strategy in amphisbaenians (Gans 1968). Amphisbaenian species that exhibit this side-to-side rotation tend to have a laterally compressed, wedge-like snout (Gans 1968), rather than the arbitrary, bullet-shaped head used here.

The overall reduction in peak force might explain the mechanical limitations of the penetration trials in chapter 3. In the case of the robotic penetrator, it seemed that the lower amplitude trials in sand pushed the limits of the mechanical capability of the machine more so than higher amplitudes. A similar effect might influence the burrowing strategy of amphisbaenians. Even if total work increases through head movements, biological constraints might make it impossible for the organism to penetrate at all unless the peak force required is sufficiently lowered. Finally, the experiments in this chapter tested only a limited set of head oscillation parameters. Other oscillation ratios or amplitudes might have a significant reduction in force and work. Deufel (2017), for example, noted that the burrowing snake *Aspidelaps scutatus* employed side-to-side head movements of approximately 32 degrees, while Sharpe et al. (2015) recorded oscillations of only about 4.5 degrees but at a frequency of 2-4 cycles per second, indicating that there is a wide range of parameters used by organisms. Also, it is possible that the formation of tunnel walls could work differently if the head is oscillating from side to side while simultaneously pushing forward, and a different effect would be seen if the oscillation occurs as a separate step. This last possibility will be investigated in chapter 5.

CHAPTER V

THE EFFECT OF INTERMITTENCY ON FORCES AND WORK REQUIRED FOR BURROWING

Introduction

Rotational movements have been found to decrease penetration forces (Tang et al., 2024; Tang & Tao, 2022), possibly through crack propagation or disruption of force chains (Dorgan et al., 2005; Tang et al., 2024; Tang & Tao, 2022). Burrowing organisms may use oscillatory head movements as a means of excavation or tunnel formation in granular media as well (Deufel, 2017;Sharpe et al., 2015; Gans 1968; Gans 1978) Amphisbaenians reportedly exhibit either the simultaneous push-rotate movement of the head, or the decoupled rotate-push-rotate movement (Gans 1968; Gans 1978; Bergman and Berry 2021). Alternatively, amphisbaenians will omit the head rotations altogether in looser soil (Gans 1968). The reason that the push and the oscillation are sometimes decoupled is uncertain. Gans suggested that decoupling the head rotation from the forward push leads to a further reduction in required force, partly because the relationship between force and acceleration (force = mass*acceleration) implies that multiple rapid burst of movement would impart a higher force to the substrate than one continuous push (Gans 1968). However, this hypothesis has not been tested. In chapter 4 of this thesis, I found no significant decrease in penetration forces associated with a simultaneous head movement/forward penetration coupling. Sharpe et al. (2015) found a decrease in drag force following the rotation of a cylindrical intruder, the effect of which was transient. It is possible that head oscillation during forward penetration (as opposed to preceding it) interacts with the substrate in a different way than it might if it were stationary. For example, a side-to-side oscillating head is changing the geometry and surface area of the leading segment of the penetrator, which could cause changes in penetration forces that would not be seen in stationary oscillating head. If this is the case, a stationary oscillation phase followed by a forward push phase might be more advantageous. As Sharpe et al. (2015) found, such an oscillation phase has only a transient effect, requiring more phases of oscillation to continue this force reduction.

In this chapter, I investigate the hypotheses that (1) decoupling the head rotation from the forward penetration will cause a significant decrease in peak penetration force and total work for shaft penetration when compared to a control group with no head movement, and (2) considering that experiments have indicated a transient decrease in drag force following rotation (see Sharpe et al. 2015), there will be a significant difference between trials when the distance between head oscillation phases is varie

Methods

This chapter used the same robotic model described in the methods and used for chapters 3 and 4. The shaft and the head were reprogrammed so that the head and shaft movements occurred separately. For each amplitude, an oscillation of the head was performed, followed by an extension of the shaft, this sequence repeated one or more times depending on the strategy employed. Extension distances included 2cm, 4cm, and 8cm between rotations (a distance of 8cm meaning that only one repetition of head movements took place, before a single forward push). This was done for amplitudes of 5, 10, and 15 degrees, and for head oscillations of 1 and 2 per oscillation phase (i.e. between pushes). There was also a control set with no head movement, and only a single continuous push. 3-way ANOVAs were done to compare all variables with fixed factors of oscillation number (i.e., the number of times that the head rotated between pushes), amplitude, and distance between head oscillation phases, in a fully crossed design. Again, missing degrees of freedom associated with a zero value for oscillation number, amplitude, and distance between oscillation phases prevented 3-way ANOVAs to include the controls, so peak shaft force and total shaft work were compared between each trial set and the control were compared through Tukey's HSD. The results of the ANOVAs for the shaft data are shown in tables 27 and 28. Differences between conditions within an effect which was significant were assessed using Tukey's Honest Significant Difference, the results of which are shown in tables 29 and 32. The results of the Tukey's HSD comparisons with the control groups are shown in tables 33-38.

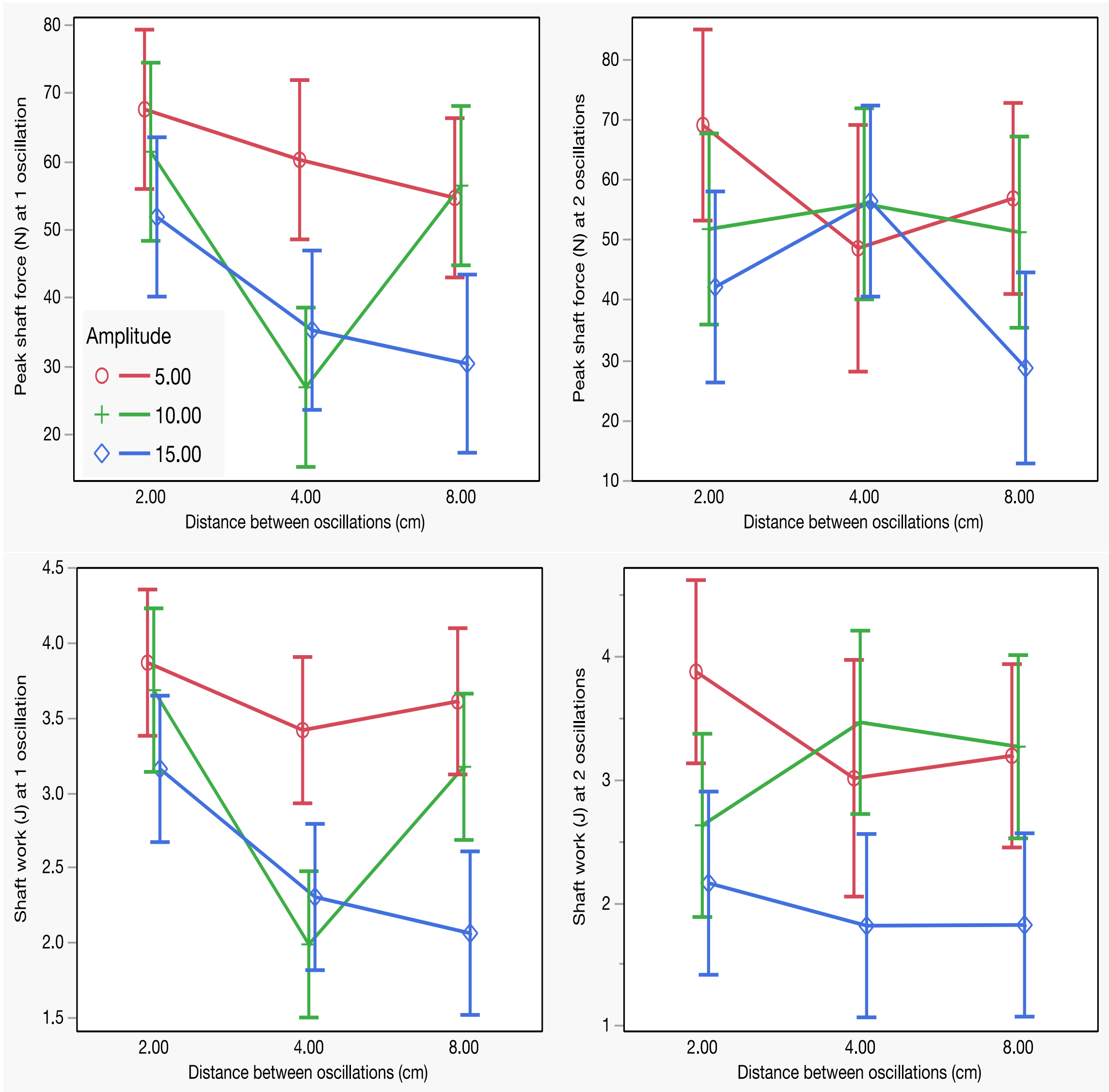

Figure 2: The relationship of number of oscillations and distance between oscillation phases on the peak shaft force and total shaft work at amplitudes of 5, 10, and 15 degrees. Error bars represent the 95% confidence interval.

Table 27: Results of 3-way ANOVA comparing peak shaft force between experimental groups

Variable	F	dF	P
Peak shaft force			
Whole model	3.31	**17,68**	**0.0002**
Amplitude	10.40	**2,68**	**0.0001**
Oscillation number	0.29	1,68	0.59
Amplitude*oscillation number	0.45	2,68	0.64
Distance between oscillations	4.49	**2,68**	**0.0147**
Amplitude*Distance between oscillations	2.23	4,68	0.07
Oscillations*Distance between oscillations	2.84	2,68	0.07
Amplitude*Oscillations*Distance between oscillations	2.20	4,68	0.08

Table 28: Results of 3-way ANOVA comparing total shaft work between experimental groups (control not included)

Variable	F	dF	P
Total shaft work			
Whole model	5.24	**17,68**	**< 0.0001**
Amplitude	24.43	**2,68**	**< 0.0001**
Oscillation number	2.23	1,68	0.14
Amplitude*Oscillation number	2.14	2,68	0.13
Distance between oscillations	4.80	**2,68**	**0.0113**
Amplitude*Distance between oscillations	0.87	4,68	0.48
Oscillations*Distance between oscillations	2.80	2,68	0.07
Amplitude*Oscillations*Distance between oscillations	3.01	**4,68**	**0.0241**

Table 29: Results of Tukey's HSD test comparing peak shaft force by amplitude

Amplitude	-Amplitude	Difference	Std. Error	T Ratio	P-value	95% CI Lower	95% CI Upper
5	10	8.87	4.10	2.16	0.09	-0.96	18.70
5	15	18.69	4.10	4.56	**< 0.0001**	8.86	28.52
10	15	9.83	4.04	2.43	**0.0456**	0.15	19.50

Table 30: Results of Tukey's HSD test comparing total shaft work by amplitude

Amplitude	- Amplitude	Difference	Std. Error	T Ratio	P-value	95% CI Lower	95% CI Upper
5	10	0.46	0.19	2.49	**0.0403**	0.02	0.91
5	15	1.28	0.19	6.88	**< 0.0001**	0.83	1.72
10	15	0.82	0.18	4.47	**< 0.0001**	0.38	1.25

Table 31: Results of Tukey's HSD test comparing peak shaft force by distance between oscillations

Distance between oscillation	-Distance between oscillations	Difference	Std. Error	T Ratio	P-value	95% CI Lower	95% CI Upper
2	4	10.06	4.10	2.45	**0.0437**	0.23	19.89
2	8	10.92	4.04	2.71	**0.0232**	1.25	20.59
4	8	0.86	4.10	0.21	0.98	-8.97	10.69

Table 32: Results of Tukey's HSD test comparing total shaft work by distance between oscillations

Distance between oscillation	-Distance between oscillations	Difference	Std. Error	T Ratio	P-value	95% CI Lower	95% CI Upper
2	4	0.56	0.19	3.03	**0.0096**	0.12	1.01
2	8	0.37	0.18	2.05	0.1078	-0.06	0.81
4	8	-0.19	0.19	-1.01	0.57	-0.63	0.26

Table 33: Connecting letters report, peak shaft force and distance between oscillations

Level		Mean
0.00	A	49.388000
2.00	A	57.047517
4.00	A	47.029143
8.00	A	46.822138

Table 34: Connecting letters report, shaft work and distance between oscillations

Level		Mean
0.00	A	3.1520000
2.00	A	3.2088276
4.00	A	2.6375714
8.00	A	2.8771034

Table 35: Connecting letters report, peak shaft force by oscillation number

Level		Mean
0.00	A	49.388000
1.00	A	49.456744
2.00	A	51.218512

Table 36: Connected letters report for shaft work, by oscillation number

Level		Mean
0.00	A	3.1520000
1.00	A	3.0319070
2.00	A	2.7900465

Table 37: Connected letters report for peak shaft forces, by amplitude

Level			Mean
0.00	A	B	49.388000
5.00	A		60.159143
10.00	A	B	50.143724
15.00		B	41.048690

Table 38: Connected letters report for total shaft work, by amplitude

Level			Mean
0.00	A	B	3.1520000
5.00	A		3.5261429
10.00	A		3.0077931
15.00		B	2.2202069

Results

Figure 16 presents a set of 3 factor plots showing the relationships between the variables. Amplitude and distance between oscillations both had significant main effects on the peak force required by the shaft for the robot to penetrate through damp perlite (amplitude, $F_{2,68} = 10.40$, $p < 0.0001$; distance between oscillations, $F_{2,68} = 4.49$, $p = 0.0147$). Post hoc analysis through Tukey's HSD indicated that the peak shaft force declined with increased head oscillation amplitude between 5 and 15 degrees, and between 10 and 15 degrees, but not between 5 and 10 degrees (see table 29). Peak shaft force was also significantly higher at a head oscillation distance of 2cm than for a head oscillation distance of 4 cm or 8cm, though there was no significant difference between the two highest head oscillation distances (Table 30).

Likewise, ANOVA indicated that amplitude and distance between oscillations had significant main effects on the work done by the shaft during the penetration (amplitude, $F_{2,68} = 24.43$, $p = < 0.0001$; distance between oscillations, $F_{2,68} = 4.80$, $p = 0.0113$). There was a significant interaction between amplitude, number of oscillations, and the distance between oscillations on the total work of the shaft ($F_{4,68} = 3.01$, $p = 0.0241$). A Tukey's HSD test indicated that the total shaft work decreased with increasing head oscillation amplitude, with each pairwise difference being significant (table 27).

Tukey's HSD indicated no significant difference in peak shaft force or work between the test groups with either 1 or 2 oscillations and the control group, or between the distances of 2cm, 4cm, and 8cm between oscillation phases and the control group. When the control groups were included in the analysis, there was a significant decrease in peak shaft force from a head amplitude of 5 degrees to a head amplitude of 15 degrees. There was also a significant decrease in total shaft work associated with a head amplitude of 15 degrees when compared to the shaft work associated with 5 and 10 degree amplitudes, when the control group was considered.

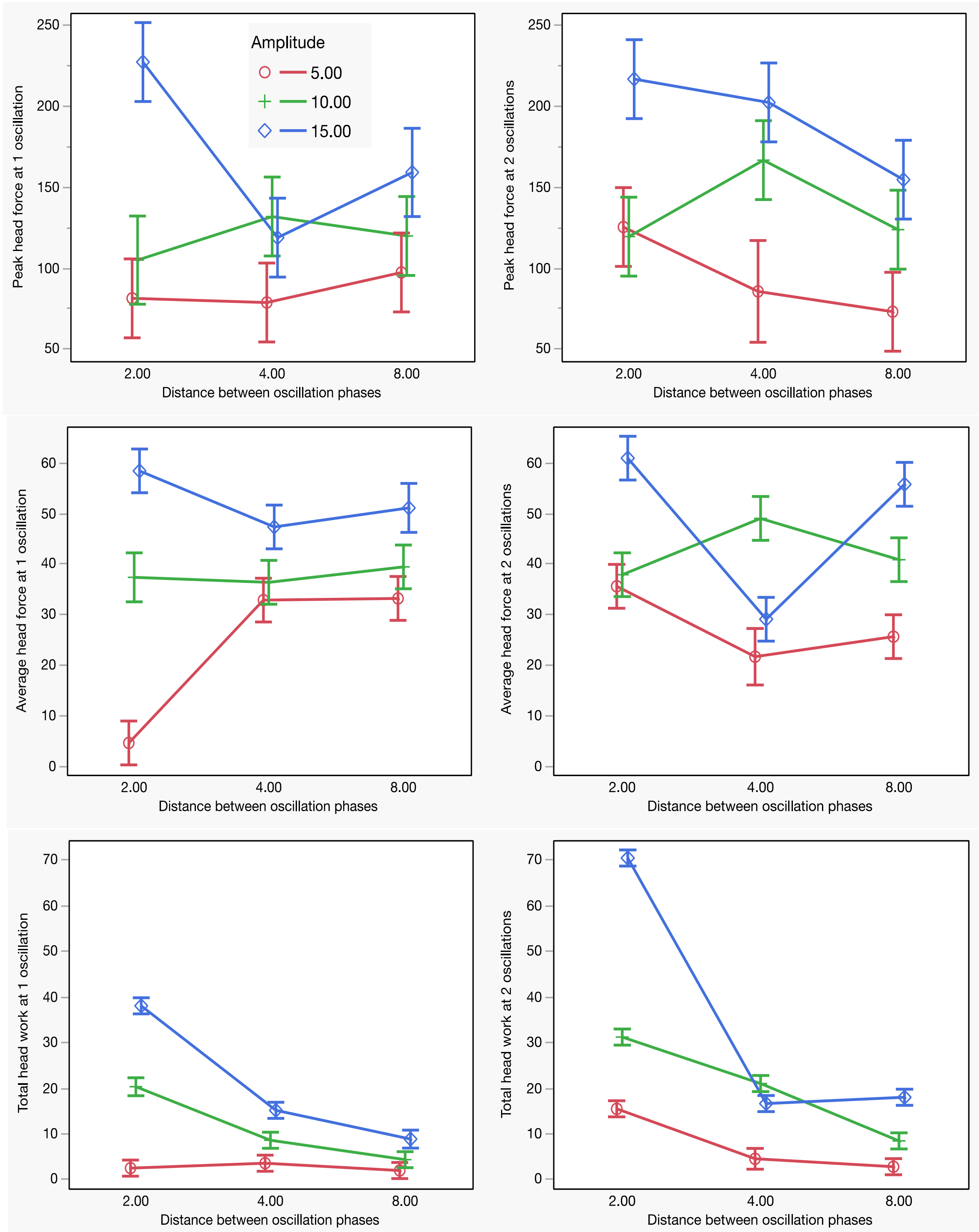

Figure 3: The relationship of number of oscillations and distance between oscillation phases on the peak shaft force and total shaft work at amplitudes of 5, 10, and 15 degrees. Error bars represent the 95% confidence interval.

Head data

Table 39: Results of 3-way ANOVA comparing peak head force between experimental groups

Variable	F	dF	P
Peak head force			
Whole model	14.21	**17,68**	**< 0.0001**
Amplitude	75.97	**2,68**	**< 0.0001**
Oscillation number	7.70	**1,68**	**0.0071**
Amplitude*oscillation number	0.46	2,68	0.63
Distance between oscillations	5.93	**2,68**	**0.0042**
Amplitude*Distance between oscillations	8.84	**4,68**	**<0.0001**
Oscillations*Distance between oscillations	5.84	**2,68**	**0.0045**
Amplitude*Oscillations*Distance between oscillations	3.70	**4,68**	**0.0088**

Table 40: Results of 3-way ANOVA comparing average head force between experimental groups

Variable	F	dF	P
Average head force			
Whole model	39.55	**17,68**	**< 0.0001**
Amplitude	184.03	**2,68**	**< 0.0001**
Oscillation number	2.75	1,68	0.10
Amplitude*oscillation number	6.79	**2,68**	**0.0020**
Distance between oscillations	7.35	**2,68**	**0.0013**
Amplitude*Distance between oscillations	27.70	**4,68**	**< 0.0001**
Oscillations*Distance between oscillations	22.60	**2,68**	**< 0.0001**
Amplitude*Oscillations*Distance between oscillations	26.45	**4,68**	**< 0.0001**

Table 41: Results of 3-way ANOVA comparing total head work between experimental groups

Variable	F	dF	P
Total head work			
Whole model	361.11	**17,68**	**< 0.0001**
Amplitude	923.34	**2,68**	**< 0.0001**
Oscillation number	484.80	**1,68**	**< 0.0001**
Amplitude*oscillation number	39.80	**2,68**	**< 0.0001**
Distance between oscillations	1026.90	**2,68**	**< 0.0001**
Amplitude*Distance between oscillations	263.06	**4,68**	**< 0.0001**
Oscillations*Distance between oscillations	117.95	**2,68**	**< 0.0001***
Amplitude*Oscillations*Distance between oscillations	41.55	**4,68**	**< 0.0001***

Table 42: Results of Tukey's HSD test comparing peak head force by amplitude

Amplitude	-Amplitude	Difference	Std. Error	T Ratio	P-value	95% CI Lower	95% CI Upper
5	10	-37.42	7.29	-5.13	**<0.0001**	-54.90	-19.94
5	15	-89.34	7.29	-12.25	**<0.0001**	-106.82	-71.86
10	15	-51.93	7.18	-7.24	**<0.0001**	-69.12	-34.73
5	10	-14.53	1.30	-11.21	**<0.0001**	-17.64	-11.43
5	15	-24.79	1.30	-19.12	**<0.0001**	-27.90	-21.69
10	15	-10.26	1.28	-8.04	**<0.0001**	-13.32	-7.20

Table 43: Results of Tukey's HSD test comparing average head force by amplitude

Amplitude	-Amplitude	Difference	Std. Error	T Ratio	P-value	95% CI Lower	95% CI Upper
5	10	-14.53	1.30	-11.21	**<0.0001**	-17.64	-11.43
5	15	-24.79	1.30	-19.12	**<0.0001**	-27.90	-21.69
10	15	-10.26	1.28	-8.04	**<0.0001**	-13.32	-7.20

Table 44: Results of Tukey's HSD test comparing total head work by amplitude

Amplitude	-Amplitude	Difference	Std. Error	T Ratio	P-value	95% CI Lower	95% CI Upper
5	10	-10.52	0.53	-19.85	**<0.0001**	-11.79	-9.25
5	15	-22.74	0.53	-42.89	**<0.0001**	-24.01	-21.47
10	15	-12.21	0.52	-23.42	**<0.0001**	-13.46	-10.97

Table 45: Results of Tukey's HSD test comparing peak head force and total head work by number of oscillations per oscillation phase (no significant interaction was found between number of oscillations and average head force)

Variable	Oscillation	-Oscillation	Difference	Std. Error	T Ratio	P-value	95% CI Lower	95% CI Upper
Peak head force	1	2	-16.44	5.92	-2.78	**0.0071**	-28.26	-4.62
Total head work	1	2	-9.48	0.43	-22.02	**<0.0001**	-10.34	-8.62

Table 46: Results of Tukey's HSD test comparing peak head force by distance between oscillation phases

Distance between oscillations	-Distance between oscillations	Difference	Std. Error	T Ratio	P-value	95% CI Lower	95% CI Upper
2	4	15.14	7.29	2.08	0.10	-2.34	32.62
2	8	24.50	7.18	3.41	**0.0031**	7.31	41.70
4	8	9.36	7.29	1.28	0.41	-8.12	26.84

Table 47: Results of Tukey's HSD test comparing average head force by distance between oscillation phases

Distance between oscillations	-Distance between oscillations	Difference	Std. Error	T Ratio	P-value	95% CI Lower	95% CI Upper
2	4	3.07	1.30	2.37	0.05	-0.03	6.18
2	8	-1.86	1.28	-1.46	0.32	-4.92	1.20
4	8	-4.93	1.30	-3.80	**0.0009**	-8.04	-1.83

Table 48: Results of Tukey's HSD test comparing total head work by distance between oscillation phases

Distance between oscillations	-Distance between oscillations	Difference	Std. Error	T Ratio	P-value	95% CI Lower	95% CI Upper
2	4	18.10	0.53	34.15	**<0.0001**	16.83	19.38
2	8	22.29	0.52	42.74	**<0.0001**	21.04	23.54
4	8	4.18	0.53	7.89	**<0.0001**	2.91	5.45

Table 49: Mean peak force and work for the head and shaft at amplitudes of 0, 5, 10, and 15 degrees

	0 degrees	5 degrees	10 degrees	15 degrees
Peak force				
Head	0	90.19	128.07	179.92
Shaft	49.39	60.16	50.14	41.05
Total	49.39	150.35	178.21	220.97
Total work				
Head	0	5.03	15.35	28.38
Shaft	3.15	3.53	3.01	2.22
Total	3.15	8.56	18.36	30.6

Table 50: Mean peak force and work for the head and shaft at 2cm, 4cm, and 8cm between oscillation phases, and 0cm (no oscillation phase)

	0cm	2cm	4cm	8cm
Peak force				
Head	0	146.74	133.40	119.53
Shaft	49.39	56.46	47.03	46.82
Overall	49.39	203.20	180.43	166.35
Total work				
Head	0	29.86	11.94	7.20
Shaft	3.15	3.17	2.64	2.88
Total work	3.15	33.03	14.58	10.08

Figure 17 presents a set of 3 factor graphs showing the peak forces, average forces, and total work experienced by the head of the robot for the different parameters of amplitude, number of oscillations per oscillation phase, and distance between oscillation phases. Amplitude, number of oscillations, and distance between oscillation phases had significant main effects on the peak force experienced by the head (amplitude, $F_{2,68} = 75.97$, $p < 0.0001$; number of oscillations, $F_{1,68} = 7.70$, $p < 0.0071$; distance between oscillation phases, $F_{2,68} = 5.93$, $p = 0.0042$), Post hoc analysis through Tukey's HSD indicated that the peak head forces increased with increasing head oscillation amplitude with each pairwise difference being significant (see table 42). Tukey's HSD also revealed that the peak head forces experienced by the head during a 1-oscillation phase were significantly lower than those experienced during a 2-oscillation phase (see table 45). The peak forces experienced by the head with a 2cm distance between oscillation phases were significantly higher than those experienced by the head with an 8cm distance between oscillation phases (see table 46).

Amplitude of oscillation and the distance between oscillation phases had a significant effect on the average head force (amplitude, $F_{2,68} = 184.03$, $p < 0.0001$; distance between oscillation phases, $F_{2,68} = 7.35$, $p = 0.0013$). Tukey's HSD showed that the average head force increased with increasing amplitude, with each pairwise difference being significant (see table 43). The average head force at a 4cm distance between oscillation phases was significantly lower than the average head force at an 8cm distance between oscillation phases (see table 47).

Amplitude, number of oscillations, and distance between oscillation phases had significant main effects on the total work done by the head (amplitude, $F_{2,68} = 923.34$, $p < 0.0001$; number of oscillations, $F_{1,68} = 484.80$, $p < 0.0001$; distance between oscillation phases, $F_{2,68} = 1026.90$, $p < 0.0001$) There was a significant interaction between amplitude and the oscillation number on the total head work ($F_{2,68} = 39.80$, $p < 0.0001$), a significant interaction between amplitude and distance between oscillation number on total head work ($F_{4,68} = 263.06$, $p < 0.0001$), a significant interaction between oscillation number and distance between oscillation phases on total head work ($F_{2,68} = 117.95$, $p < 0.0001$) and a significant interaction between amplitude, oscillation number, and distance between oscillation phases on total head work ($F_{4,68} = 41.55$, $p < 0.0001$). Tukey's HSD revealed that the total head work increased with increasing amplitude, with each pairwise difference being significant (see table 44). Total head work done at an oscillation number of 1 was significantly lower than that done at an oscillation number of 2 (see table 45). Tukey's HSD indicated that the total head work increased with distance between oscillation phases, with each pairwise difference being significant.

Discussion

The fact that an increased amplitude leads to an increase in the peak and average forces experienced by the rotating head, may reflect the fact that the head is moving a greater distance and therefore dealing with a larger amount of material. Similarly, total head work may increase significantly with an increase in amplitude ($p < 0.0001$) for the same reason. This is somewhat complicated by the interactions between parameters however, as can be seen above.

The peak force increases significantly with an increase in oscillation number ($p = 0.0071$), while the average force does not ($p = 0.10$). Total head work increases significantly, which is not surprising because 2 oscillations per oscillation phase means that the head is rotating twice as much as 1 oscillation per oscillation phase. A possible explanation for the increase in peak force with a 2-oscillation phase could be that loose material collapses from the roof and/or walls of the excavated cavity after the first sweep, causing the second sweep to have to compact more material into a previously compacted wall.

When the head completes an oscillation phase every 2cm, the peak force on the head increases significantly ($p = 0.0031$) compared to the 8cm distance (where the oscillation phase begins the sequence, followed by a single continuous push). The peak force on the head at a distance between oscillation phases of 4cm appears to be intermediate between that experienced by the head at 2cm and 8cm, and is not significantly different from either. Because of the history dependence properties of damp granular media (Schiebel et al., 2020), it could be that the head rotations, when occurring at a distance of 2cm from one another, are packing material into an area that had been compacted by the previous head sweep. Since granular media is subject to jamming (Stone et al., 2004; Kang et al. 2018), another possibility is that the head rotations occurring after the movement of the shaft (as would happen for the second phase of the 4cm distance and all but the first of the 2cm distance) are taking place into material that has been jammed by the forward motion of the shaft. The average force follows a somewhat different trend, increasing significantly from a distance of 4cm to a distance of 8cm ($p = 0.0009$), but showing no significant difference between the average force at a distance of 2cm to either that of a 4cm or 8cm distance. Overall, the average head force does not show a clear, consistent trend (see figure 17).

There is an overall decrease in peak shaft force associated with the increased amplitude of the head sweeps after an amplitde of 5 degrees, though the difference is only significant between 5 and 15 degrees. There is a decrease in shaft work at a head amplitude of 15 degrees when compared to 5 and 10 degree amplitudes. This suggests the possibility that more material is being excavated in front of the intruder when the head is making a wider sweep. For amplitudes of 5 and 15 degrees, the decrease in shaft peak force appears to be consistent with an increase in amplitude, for distances of 2cm and 8cm between oscillation phases. The exception is the peak shaft force at a distance of 4cm and a head oscillation number of 2. At an amplitude of 10 degrees, the trend is much less linear. At one oscillation, both peak shaft force and work decrease sharply from a distance between oscillation phases of 8cm to 4cm, and then rise again at a distance between oscillations of 2cm.

A possible explanation is that there are competing effects on force and work. Increasing amplitude decreases shaft peak force and work overall, but as mentioned above damp granular media is subject to hysteresis (Schiebel et al., 2020) and there may be some interactions with packed media from the previous head oscillation when the penetrator is making these head movement phases closer together. Possibly, material is being pushed into the previously packed wall and causing it to buckle inward. This would also explain the increase of force and work experienced by the head. The region just behind the head of the robot, while covered with a plastic skin, left a small gap between the head and the shaft so that the head could rotate. This left a space that could, under pressure, be buckled inward.

At a lower head amplitude of 5 degrees, there might be less of this interaction, while at the higher amplitudes there may be more of an interaction. However, the increase in the force and work experienced by the shaft as a result of this interaction might be offset by the larger excavation made by higher head amplitudes. An amplitude of 15 degrees might cause a large enough advantage to counteract the loss entirely, while an amplitude of 10 degrees might be too high to avoid it but not high enough to counteract it at the lowest distance (2cm) between oscillations.

Number of head oscillations had no significant direct effect either on peak shaft force or on total shaft work, suggesting that one sweep of the head is enough to excavate a cavity and that more than one is unnecessary. The effect of distance between oscillation phases on shaft forces and work is more complicated, as it was with the head data. Peak shaft forces at distances of 2cm and 4cm were significantly different from one another, and those at distances of 2cm and 8cm were significantly different from one another. However, there is no significant difference between the peak forces of the control group and any of the distances. Total shaft work is only significantly different between distances of 2cm and 4cm. A possible explanation for this nonlinearity could be the same competing interactions mentioned above.

Because of the increase in force and work that occurs with a decreasing distance between head oscillations, there may be a minimum distance between oscillation phases below which there is no advantage in the strategy in terms of force or work reduction for an organism with a similar body plan. This could relate to the geometry of the rotating head. The head of the robot in this case had a length of 7.5cm from base to tip. A shorter head might allow for shorter distances between oscillations without there being an interaction between newly excavated and previously excavated substrate. Also, a narrower head would push less material backwards than the bullet-shaped head here, which expands in width from tip to base.

When the force and work of the head and shaft are taken together, it can be seen that head movements in all cases lead to a total increase of the peak force and the total work of the push. As mentioned in chapter 3, this could be related to the specific head geometry of the robot used here. In theory, a head with a smaller surface area would require less force and less work to excavate the space in front of the robot, although of course there would be a consequent decrease in the amount of material excavated. Penetration forces are sensitive to geometry (Bergmann and Berry 2021; Mishra et al. 2018), and as mentioned earlier, amphisbaenians appear to have specific geometries correlated with specific oscillation strategies (Gans 1968). This suggests that a general bullet-shaped head does not experience the same interactions with the media as a burrowing organism with a wedge-shaped head employing the side-to-side oscillationstrategy. This would be an interesting area for future study.

CHAPTER VI

CONCLUSION

While different substrates will probably always exhibit slightly different mechanical properties due to differences in particle shape and size (Bergmann & Berry 2021), the more lightweight and less logistically problematic crushed expanded perlite may be a suitable substitute for sand in lab experiments of this type given that proper caution is taken in generalizing results. If so, this could be distinctly advantageous in performing research in the future, as the limitations of mechanical systems would be lessened and the time required for doing repeated tests would be decreased (considering that a testing area needs to be entirely emptied and re-filled for each individual trial). While perlite exhibited some differences from sand during the testing, it is uncertain to what extent it compares to other substitutes that have been used in previous research. Also, since burrowers in natural habitats encounter different substrate types worldwide, it raises some questions about the generalizability of data across these habitats. Differences between the mechanics of the robot's penetration through perlite and sand could suggest mechanical differences that burrowers experience, and thus explain changes in strategy noticed in some individual amphisbaenians (see Gans 1960). Alternatively, it could represent a scaling effect that is not apparent at smaller amplitudes for head movements in perlite. There is a need for research investigating the reasons for differences in substrate behavior at a physical level, a specific area of focus being the sudden transition to higher forces in sand with an increased amplitude of head movements.

In the case of this robophysical model, head movement doesn't seem to help in penetration when looking at the forces and work involved overall (that is, the sum of force and work including both head and shaft). In the few conditions in which head movement does reduce shaft force or work, the benefit is not enough to compensate for the force and work needed to move the head. This could suggest that the head movements mimicked here are employed by organisms for reasons other than force or work reduction in burrowing, such as sensing areas of varied compaction in the soil through which they are moving (Sharpe et al. 2015), hunting prey (Gans 1968), or constructing permanent tunnels for later use (Gans 1968). Amphisbaenians are known to construct permanent tunnels (Gans 1968) and the advantages of having done so may be so great that the initial cost of construction is negligible. A permanent tunnel may be necessary for some activities, such as respiration and foraging (Gans 1968; Lowie et al. 2021). Furthermore, a permanent tunnel can be re-used. Any cost involved in constructing a given length of a tunnel would become less in proportion to the advantages gained each time that section of tunnel is used. Therefore, the selective pressures on an organism might be more closely related to its overall *ability* to construct the tunnel (i.e., being able to generate enough force) rather than optimizing the effort required to do so. These factors could have implications in terms of bio-inspiration, and would serve as a further caution that patterns observed in nature do not always confer an obvious engineering advantage from a human standpoint (Martinez et al. 2022).

Also, the side-to-side head movements explored in this thesis have been observed to occur specifically among those amphisbaenians with a laterally flattened keel-shaped head, and not among those with differently shaped skulls like the rounded shape here (Gans 1974; Hawkins et al. 2022). Moreover, the keel shape and side-to-side combination has developed among species of different clades of amphisbaenians independently (Hawkins et al. 2022), which suggests the likelihood of some clear advantage to the morphology-kinematic coupling. I would hypothesize that a distinct side-to-side strategy is not employed by amphisbaenians that do not have this specifically shaped head because this strategy is not advantageous when not paired with the specific head shape. An investigation into head geometry and kinematic strategies would be a very interesting area of future study. The experiments conducted here, in addition to employing only one (non-biologically-inspired) head shape, also tested a limited range of the conceivable kinematics (i.e. three head oscillation amplitudes, two oscillation ratios, and three distances between oscillation phases). Meanwhile, the amount of moisture content in the substrates was not varied, leaving questions about how these variables would play out at other degrees of moisture. Investigations exploring other ranges of these variables are warranted.

The hydraulically-actuated robophysical model used here is, to the best of my knowledge, a unique design for burrowing experiments. It has advantages for submerged burrowing experiments, as described in chapter 2. However, a hydraulic mechanism comes with unique limitations. One such limitation is that any leakage of hydraulic fluid causes the force transfer to deviate from the ideal 1:1 relationship. While leakage was monitored and corrected for as much as possible, the possibility of tiny, unnoticed leakage occurring cannot be entirely ruled out. For the trials involving simultaneous head motion coupled with shaft penetration, leakage could lead to a degree of uncertainty in the oscillation ratio (for example, if the shaft were lagging slightly because of air in the system). A similar limitation is inherent with physical compliance in the components used, and with changes in fluid viscosity based on temperature fluctuations. Limitations such as this should be considered in the future if a similar hydraulically-actuated robot is employed. Feedback from a potentiometer corrects for such uncertainty in the rotation of the head, but a similar feedback system for the shaft could be helpful.

A similar limitation has to do with the uncertainty surrounding the mechanics of wet granular media. The motor settings required to temporally synchronize the head and the shaft, in the case of simultaneous head rotation-shaft penetration trials, had to be determined experimentally. Proper synchronization assumes that the substrate mechanics were the same for each trial. Any fluctuations in the mechanics of the substrate (such as pockets of higher density) could possibly influence the timing of shaft or head movements. The sieving technique was intended to prevent such inhomogeneity, and such fluctuations in timing noticed during the trials were small (+/- approximately 2s). But a solution to correct for this would be desirable in future experiments.

The hydraulic system used here can serve as a starting point for other robophysical models that need to transfer large forces to a penetrator with a limited diameter, and with a high degree of accuracy. Use of an electric motor in the robotic penetrator itself would be impractical without significantly scaling up the size of the robot and thus increase the required forces. A pneumatic system might avoid this, but because of the compressibility of air would make it difficult to determine the position of the robot while submerged. An alternative model might be used in which the penetrator is suspended from an arm attached perpendicularly to the shaft to a driving mechanism above (as in Sharpe et al. 2015), but this would change the geometry of the intruder. Because of the cohesiveness of damp media, such a change in geometry could have a significant influence on the outcome.

Pieces of the mechanism that were under high loads during operation (such as the gear train, load cells, and connecting pieces between the load cells and pistons) were the most susceptible to failure during this process. These could be replaced with metal pieces in the future: metal gears and load cells, and possibly custom-machined or cast pieces for connecting pieces. This might enable a larger scope of parameters to be tested. It is vital to use the proper hydraulic tubing to connect driving and actuating pistons. In addition to adding unnecessary compliance and therefore inaccuracy to the system, I found that using tubing with too low of a pressure rating lead to an expansion around the couplings on the pistons that allowed small leaks to occur over time. Once the proper tubing was determined (which can be done through a calculation of the pressure in the system), these leaks were greatly minimized. Once the proper tubing is selected and suitably durable materials are found for components, the force output of the machine could theoretically be greatly increased by adding more gears to the gear train (although doing so would also greatly decrease the speed at which the machine operates). The diameter of the robot was constrained by the diameter of commercially available pistons. It is possible that custom-machined pistons of a smaller diameter could be used, thus allowing for a smaller robotic penetrator.

Nonetheless, in its current state the robot is capable of generating high forces, and can be tuned for a versatile range of testing. Heads can be easily removed and replaced, allowing for tests of different head morphologies and different morphology/kinematic couplings (such as side-to-side head oscillations coupled with a wedge-shaped head). The robot can be reoriented to test head oscillations in different axes (for example, vertical rather than horizontal head movements). Different oscillation patterns can be programmed besides those examined here. The flexible plastic sheathing covering the robot could be replaced to explore the results of different skin types (for example, different coefficients of friction related to different materials, or different morphologies using a combination of 3D printing and silicone molds). The same model can also be used as-is to explore dry substrates, and different soil types. Finally, the robot is a simplified model of a limbless, burrowing squamate. In this case, I used it to explore hypotheses concerning amphisbaenians, but it could be used to explore hypotheses concerning other organisms of a similar body plan as well.

Throughout this thesis, important questions regarding the physics of locomotion through granular media and the biology of amphisbaenians and similar burrowers have been raised, providing intriguing directions for future research. For example, the lack of reduction in force and work overall may point to alternative hypotheses concerning the purpose of the side-to-side behavior. Or, it could indicate that the kinematic strategy alone is not an advantageous behavior, and that a specific head shape is required for force or work reduction. Exploration of this second area could indicate future directions for bioinspired engineering. Additionally, the investigation of morphology-kinematic combinations such as this could help to shed light on biological questions concerning squamates. For example, the phylogeny of amphisbaenians is not fully understood, either in their relation to squamata as a whole, or in their relation to other members of the clade (de Fraga et al., 2022; Kearney, 2003). Part of the difficulty is the homoplasy of features such as head shape (de Fraga et al., 2022; Kearney, 2003), and molecular data has confirmed that distinct skull shapes are indeed often homoplastic in amphisbaenians (Kearney, 2003.; Mott & Vieites, 2009). Thus, it is uncertain which morphologies are basal. Gathering data concerning the evolutionary advantage of specific head morphologies and behaviors might help in determining specialization among lineages.

Overall, my thesis works toward advancing our understanding of burrowing in damp granular media by limbless squamates, more specifically by testing hypotheses concerning amphisbaenian behavior. These are neglected areas of inquiry. The use of lightweight perlite as a testing substrate could make experimentation with wet granular media more accessible for laboratory research, although the results of this thesis suggest that caution be used when interpreting results across different substrates. Overall, the robot constructed and used here was demonstrated to be useful for gathering data, and can be a starting point for a variety of areas of future research.

REFERENCES

Agarwal, S., Goldman, D. I., & Kamrin, K. (2023). Mechanistic framework for reduced-order models in soft materials: Application to three-dimensional granular intrusion. Proceedings of the National Academy of Sciences of the United States of America, 120(4), 1–12. https://doi.org/10.1073/pnas.2214017120

Aguilar, J., Zhang, T., Qian, F., Kingsbury, M., McInroe, B., Mazouchova, N., Li, C., Maladen, R., Gong, C., Travers, M., Hatton, R. L., Choset, H., Umbanhowar, P. B., & Goldman, D. I. (2016). A review on locomotion robophysics: The study of movement at the intersection of robotics, soft matter and dynamical systems. Reports on Progress in Physics, 79(11). https://doi.org/10.1088/0034-4885/79/11/110001

Ameratunga, J., Sivakugan, N., & Das, B. M. (2016). Developments in Geotechnical Engineering Correlations of Soil and Rock Properties in Geotechnical Engineering. http://www.springer.com/series/13410

Astley, H. C., Mendelson, J. R., Dai, J., Gong, C., Chong, B., Rieser, J. M., Schiebel, P. E., Sharpe, S. S., Hatton, R. L., Choset, H., & Goldman, D. I. (2020). Surprising simplicities and syntheses in limbless self-propulsion in sand. Journal of Experimental Biology, 223(5), 1–12. https://doi.org/10.1242/jeb.103564

Augé, M. L. (2012). Amphisbaenians from the European Eocene: A biogeographical review. Palaeobiodiversity and Palaeoenvironments, 92(4), 425–443. https://doi.org/10.1007/s12549-012-0104-6

Aydin, Y. O., Rieser, J. M., Hubicki, C. M., Savoie, W., & Goldman, D. I. (2019). Physics approaches to natural locomotion: Every robot is an experiment. In Robotic Systems and Autonomous Platforms (pp. 109–127). https://doi.org/10.1016/b978-0-08-102260-3.00006-8

Bergmann, P. J., & Berry, D. S. (2021). How head shape and substrate particle size affect fossorial locomotion in lizards. Journal of Experimental Biology, 224(11). https://doi.org/10.1242/JEB.242244

Bergmann, P. J., & Morinaga, G. (2019). The convergent evolution of snake-like forms by divergent evolutionary pathways in squamate reptiles*. Evolution, 73(3), 481–496. https://doi.org/10.1111/evo.13651

Bergmann, P. J., Pettinelli, K. J., Crockett, M. E., & Schaper, E. G. (2017). It's just sand between the toes: How particle size and shape variation affect running performance and kinematics in a generalist lizard. Journal of Experimental Biology, 220(20), 3706–3716. https://doi.org/10.1242/jeb.161109

Bergmann, P. J., Mann, S. D. W., Morinaga, G., Freitas, E. S., & Siler, C. D. (2020). Convergent evolution of elongate forms in craniates and of locomotion in elongate squamate reptiles. Integrative and Comparative Biology, 60(1), 190–201. https://doi.org/10.1093/icb/icaa015

Calderón, A. A., Ugalde, J. C., Chang, L., Cristóbal Zagal, J., & Pérez-Arancibia, N. O. (2019). An earthworm-inspired soft robot with perceptive artificial skin. Bioinspiration and Biomimetics, 14(5). https://doi.org/10.1088/1748-3190/ab1440

Che, J., & Dorgan, K. M. (2010). It's tough to be small: Dependence of burrowing kinematics on body size. Journal of Experimental Biology, 213(8), 1241–1250. https://doi.org/10.1242/jeb.038661

Cho, G.-C., Dodds, J., & Santamarina, J. C. (2006). Particle Shape Effects on Packing Density, Stiffness, and Strength: Natural and Crushed Sands. https://doi.org/10.1061/ASCE1090-02412006132:5591

Coad, M. M., Blumenschein, L. H., Cutler, S., Zepeda, J. A. R., Naclerio, N. D., El-Hussieny, H., Mehmood, U., Ryu, J.-H., Hawkes, E. W., & Okamura, A. M. (2019). Vine Robots. IEEE Robotics & Automation Magazine, 27(3), 120–132. https://doi.org/10.1109/mra.2019.2947538

de Fraga, R., P. Santos-Jr, A., P. Werneck, F., C. Costa, H., T. Guimarães, J., Perez, R., Graboski Mendes, R., Mott, T., Vaz-Silva, W., & Ribeiro, S. (2022). The overlooked underground diversity: physical and chemical edaphic structure predict morphological variation in South American amphisbaenians (Squamata: Amphisbaenidae). Studies on Neotropical Fauna and Environment. https://doi.org/10.1080/01650521.2022.2147046

Del Dottore, E., Mondini, A., Sadeghi, A., Mattoli, V., & Mazzolai, B. (2018). An efficient soil penetration strategy for explorative robots inspired by plant root circumnutation movements. Bioinspiration and Biomimetics, 13(1). https://doi.org/10.1088/1748-3190/aa9998

Deufel, A. (2017). Burrowing with a kinetic snout in a snake (Elapidae: Aspidelaps scutatus). Journal of Morphology, 278(12), 1706–1715. https://doi.org/10.1002/jmor.20743

Dorgan, K. M., Jumars, P. A., Johnson, B., Boudreau, B. P., & Landis, E. (2005). Burrow extension by crack propagation. Nature, 433(7025), 475. https://doi.org/10.1038/433475a

Dorgan, K. M. (2010). Environmental Constraints on the Mechanics of Crawling and Burrowing Using Hydrostatic Skeletons. Experimental Mechanics, 50(9), 1373–1381. https://doi.org/10.1007/s11340-010-9399-2

Dorgan, K. M. (2015). The biomechanics of burrowing and boring. Journal of Experimental Biology, 218(2), 176–183. https://doi.org/10.1242/jeb.086983

Ducey, P.K., Formanowicz, Jr., D.R., Boyet, L., Mailloux, J., & Nussbaum, R.A. (1993). Experimental examination of burrowing behavior in caecilians (Amphibia: Gymnophiona): effects of soil compaction on burrowing ability of four species. Herpetologica, 49(4), 450–457. http://www.jstor.org/discover/10.2307/3892639?uid=2&uid=4&sid=21106554007093%5Cnhttp://www.jstor.org/discover/10.2307/3892639?uid=2&uid=4&sid=21106554991343

Dorgan, K. M., & Daltorio, K. A. (2023). Fundamentals of burrowing in soft animals and robots. In Frontiers in Robotics and AI (Vol. 10). Frontiers Media S.A. https://doi.org/10.3389/frobt.2023.1057876

Evans, K. M., Larouche, O., West, J. J. L., Gartner, S. M., & Westneat, M. W. (2023). Burrowing constrains patterns of skull shape evolution in wrasses. Evolution and Development, 25(1), 73–84. https://doi.org/10.1111/ede.12415

Gamel, K. M., Pinti, S., & Astley, H. C. (2024). Design of A Highly Sensitive, Low-cost Underwater Force Plate to Record Substrate Reaction Forces. Integrative Organismal Biology, 6(1). https://doi.org/10.1093/iob/obae008

Gans, C. (1960). STUDIES ON AMPHISBAENIDS (amphisbaenia, reptilia): 1. A taxonomic revision of the trogonophinae, and a functional interpretation of the amphisbaenid adaptative pattern. Bulletin of the American Museum of Natural History, 119, 1–82.

Gans, C. (1968). Relative Success of Divergent Pathways in Amphisbaenian Specialization Author (s): Carl Gans Source : The American Naturalist , Vol . 102 , No . 926 (Jul . - Aug ., 1968), pp . 345-362 Published by : The University of Chicago Press for The American So. 102(926), 345–362.

Gans, C. (1978). The characteristics and affinities of the Amphisbaenia. The Transactions of the Zoological Society of London, 34(4), 347–416. https://doi.org/10.1111/j.1096-3642.1978.tb00376.x

Gao, Z., Shi, Q., Fukuda, T., Li, C., & Huang, Q. (2019). An overview of biomimetic robots with animal behaviors. Neurocomputing, 332, 339–350. https://doi.org/10.1016/j.neucom.2018.12.071

Germann, D. P., Schatz, W., & Hotz, P. E. (2011). Artificial bivalves - The biomimetics of underwater burrowing. Procedia Computer Science, 7, 169–172. https://doi.org/10.1016/j.procs.2011.09.012

Hawkins, R. K., Bell, C. J., Olori, J. C., & Stocker, M. R. (2022). Intraspecific variation in the cranial osteology of Diplometopon zarudnyi (Squamata: Amphisbaenia: Trogonophidae). Journal of Morphology, 283(10), 1359–1375. https://doi.org/10.1002/jmor.21508

Herrel, A., Choi, H. F., Dumont, E., Schepper, N. De, Vanhooydonck, B., Aerts, P., & Adriaens, D. (2011). Burrowing and subsurface locomotion in anguilliform fish: Behavioral specializations and mechanical constraints. Journal of Experimental Biology, 214(8), 1379–1385. https://doi.org/10.1242/jeb.051185

Herrel, A., Lowie, A., Miralles, A., Gaucher, P., Kley, N. J., Measey, J., & Tolley, K. A. (2021). Burrowing in blindsnakes: A preliminary analysis of burrowing forces and consequences for the evolution of morphology. Anatomical Record, 304(10), 2292–2302. https://doi.org/10.1002/ar.24686

Herrel, A., Choi, H. F., Dumont, E., Schepper, N. De, Vanhooydonck, B., Aerts, P., & Adriaens, D. (2011). Burrowing and subsurface locomotion in anguilliform fish: Behavioral specializations and mechanical constraints. Journal of Experimental Biology, 214(8), 1379–1385. https://doi.org/10.1242/jeb.051185

Herrel, A., & Measey, G. J. (2010). The kinematics of locomotion in caecilians: Effects of substrate and body shape. Journal of Experimental Zoology Part A: Ecological Genetics and Physiology, 313 A(5), 301–309. https://doi.org/10.1002/jez.599

Heydari, S., Johnson, A., Ellers, O., McHenry, M. J., & Kanso, E. (2020). Sea star inspired crawling and bouncing. Journal of the Royal Society Interface, 17(162). https://doi.org/10.1098/rsif.2019.0700

Hipsley, C. A., Rentinck, M. N., Rödel, M. O., & Müller, J. (2016). Ontogenetic allometry constrains cranial shape of the head-first burrowing worm lizard

Cynisca leucura (Squamata: Amphisbaenidae). Journal of Morphology, 277(9), 1159–1167. https://doi.org/10.1002/jmor.20564

Hohl, L. S. L., Loguercio, M. F. C., Buendía, R. A., Almeida-Santos, M., Viana, L. A., Barros-Filho, J. D., & Rocha-Barbosa, O. (2014). Fossorial gait patterns and performance of a shovel-headed amphisbaenian. Journal of Zoology, 294(4), 234–240. https://doi.org/10.1111/jzo.12173

Hornbaker, D. J., Albert, R., Albert A-L Barabási, I., & Schiffer, P. (1997). What keeps sandcastles standing? Pilpel, N. Manufact. Chem. Aerosol News, 387, 379–382.

Hosoi, A. E., & Goldman, D. I. (2015). Beneath our feet: Strategies for locomotion in granular media. Annual Review of Fluid Mechanics, 47, 431–453. https://doi.org/10.1146/annurev-fluid-010313-141324

Isava, M., & Winter V, A. G. (2016). Razor clam-inspired burrowing in dry soil. International Journal of Non-Linear Mechanics, 81, 30–39. https://doi.org/10.1016/j.ijnonlinmec.2015.12.005

ITIS. Retrieved [11/4/2024], from the Integrated Taxonomic Information System (ITIS) on-line database, www.itis.gov, CC0 https://doi.org/10.5066/F7KH0KBK

Kalman, H. (2021). Quantification of mechanisms governing the angle of repose, angle of tilting, and Hausner ratio to estimate the flowability of particulate materials. Powder Technology, 382, 573–593. https://doi.org/10.1016/j.powtec.2021.01.012

Kang, W., Feng, Y., Liu, C., & Blumenfeld, R. (2018). Archimedes' law explains penetration of solids into granular media. Nature Communications, 9(1), 1–9. https://doi.org/10.1038/s41467-018-03344-3

Kazi, S., & Hipsley, C. A. (2018). Conserved evolution of skull shape in Caribbean headfirst burrowing worm lizards (Squamata: Amphisbaenia). Biological Journal of the Linnean Society, 125(1), 14–29. https://doi.org/10.1093/BIOLINNEAN/BLY086

Koehl, M. A. R. (2003). Physical modelling in biomechanics. Philosophical Transactions of the Royal Society B: Biological Sciences, 358(1437), 1589–1596. https://doi.org/10.1098/rstb.2003.1350

Kearney, M. (2003). SYSTEMATICS OF THE AMPHISBAENIA (LEPIDOSAURIA:SQUAMATA) BASED ON MORPHOLOGICAL EVIDENCE FROM RECENT AND FOSSIL FORMS. https://doi.org/10.1655/0733

Knudson, R. (1999). Cultural Resource Management in Context. In Archives and Museum Informatics (Vol. 13).

Kubota, T., Nagaoka, K., Tanaka, S., & Nakamura, T. (2007). Earth-worm typed drilling robot for subsurface planetary exploration. 2007 IEEE International Conference on Robotics and Biomimetics, ROBIO, 1394–1399. https://doi.org/10.1109/ROBIO.2007.4522368

Li, C., Umbanhowar, P. B., Komsuoglu, H., Koditschek, D. E., & Goldman, D. I. (2009). Sensitive dependence of the motion of a legged robot on granular media. Proceedings of the National Academy of Sciences of the United States of America, 106(9), 3029–3034. https://doi.org/10.1073/pnas.0809095106

Li, C., Zhang, T., & Goldman, D. I. (2013). A terradynamics of legged locomotion on granular media. Science, 339(6126), 1408–1412. https://doi.org/10.1126/science.1229163

Liu, B., Ozkan-Aydin, Y., Goldman, D. I., & Hammond, F. L. (2019). Kirigami skin improves soft earthworm robot anchoring and locomotion under cohesive soil. In 2019 2nd IEEE International Conference on Soft Robotics (RoboSoft) (pp. 828-833). IEEE.

Liu, C., Wan, H., & Wang, L. (2019). Effect of movement direction on resistance force in granular media. Powder Technology, 344, 545–550. https://doi.org/10.1016/j.powtec.2018.12.023

Lopez-Arreguin, A. J. R., & Montenegro, S. (2020). Towards bio-inspired robots for underground and surface exploration in planetary environments: An overview and novel developments inspired in sand-swimmers. Heliyon, 6(6), e04148. https://doi.org/10.1016/j.heliyon.2020.e04148

Lowie, A., De Kegel, B., Wilkinson, M., Measey, J., O'Reilly, J. C., Kley, N. J., Gaucher, P., Brecko, J., Kleinteich, T., Van Hoorebeke, L., Herrel, A., & Adriaens, D. (2021). Under pressure: The relationship between cranial shape and burrowing force in caecilians (gymnophiona). Journal of Experimental Biology, 224(18). https://doi.org/10.1242/jeb.242964

Maladen, R., Ding, Y., Li, C., & Goldman, D. I. (2009). Undulatory swimming in sand: Subsurface locomotion of the sandfish lizard. Science, 325(5938), 314–318. https://doi.org/10.1126/science.1172490

Maladen, R. D., Ding, Y., Umbanhowar, P. B., & Goldman, D. I. (2011). Undulatory swimming in sand: Experimental and simulation studies of a robotic sandfish.

International Journal of Robotics Research, 30(7), 793–805. https://doi.org/10.1177/0278364911402406

Martín, J., López, P., & Salvador, A. (1991). Microhabitat Selection of the Amphisbaenian Blanus cinereus Author(s): José Martín, Pilar López and Alfredo Salvador Source: Copeia, 4(4), 1142–1146.

Martín, J., López, P., & García, L. V. (2013). Soil characteristics determine microhabitat selection of the fossorial amphisbaenian Trogonophis wiegmanni. Journal of Zoology, 290(4), 265–272. https://doi.org/10.1111/jzo.12033

Martín, J., Ortega, J., García-Roa, R., Jiménez-Robles, O., Rodríguez-Ruiz, G., Recio, P., & Cuervo, J. J. (2021). Going underground: short- and long-term movements may reveal the fossorial spatial ecology of an amphisbaenian. Movement Ecology, 9(1), 1–11. https://doi.org/10.1186/s40462-021-00253-x

Martinez, A., DeJong, J., Akin, I., Aleali, A., Arson, C., Atkinson, J., Bandini, P., Baser, T., Borela, R., Boulanger, R., Burrall, M., Chen, Y., Collins, C., Cortes, D., Dai, S., DeJong, T., Del Dottore, E., Dorgan, K., Fragaszy, R., … Zheng, J. (2022). Bio-inspired geotechnical engineering: Principles, current work, opportunities and challenges. Geotechnique, 72(8), 687–705. https://doi.org/10.1680/jgeot.20.P.170

Mazouchova, N., Umbanhowar, P. B., & Goldman, D. I. (2013). Flipper-driven terrestrial locomotion of a sea turtle-inspired robot. Bioinspiration and Biomimetics, 8(2). https://doi.org/10.1088/1748-3182/8/2/026007

Mishra, A. K., Tramacere, F., Guarino, R., Pugno, N. M., & Mazzolai, B. (2018). A study on plant root apex morphology as a model for soft robots moving in soil. PLoS ONE, 13(6), 1–17. https://doi.org/10.1371/journal.pone.0197411

Mitarai, N., & Nori, F. (2006). Wet granular materials. Advances in Physics, 55(1–2), 1–45. https://doi.org/10.1080/00018730600626065

Morinaga, G., & Bergmann, P. J. (2020). Evolution of fossorial locomotion in the transition from tetrapod to snake-like in lizards. Proceedings of the Royal Society B: Biological Sciences, 287(1923). https://doi.org/10.1098/rspb.2020.0192

Mott, T., & Vieites, D. R. (2009). Molecular phylogenetics reveals extreme morphological homoplasy in Brazilian worm lizards challenging current taxonomy. Molecular Phylogenetics and Evolution, 51(2), 190–200. https://doi.org/10.1016/j.ympev.2009.01.014

Musteata, S. (2015). Preserving archaeological remains in situ: from the legal to the practical issues. The Romanian case. In Current Trends in Archaeological

Heritage Preservation: National and International Perspectives, edited by Sergiu Musteata and Stefan Caliniuc

Navas, C. A., Antoniazzi, M. M., Carvalho, J. E., Chaui-Berlink, J. G., James, R. S., Jared, C., Kohlsdorf, T., Pai-Silva, M. D., & Wilson, R. S. (2004). Morphological and physiological specialization for digging in amphisbaenians, an ancient lineage of fossorial vertebrates. Journal of Experimental Biology, 207(14), 2433–2441. https://doi.org/10.1242/jeb.01041

Naclerio, N. D., Karsai, A., Murray-Cooper, M., Ozkan-Aydin, Y., Aydin, E., Goldman, D. I., & Hawkes, E. W. (2021). Controlling subterranean forces enables a fast, steerable, burrowing soft robot. In Sci. Robot (Vol. 6). http://robotics.sciencemag.org/

Nishikawa, K., Biewener, A. A., Aerts, P., Ahn, A. N., Chiel, H. J., Daley, M. A., Daniel, T. L., Full, R. J., Hale, M. E., Hedrick, T. L., Lappin, A. K., Nichols, T. R., Quinn, R. D., Satterlie, R. A., & Szymik, B. (2007). Neuromechanics: An integrative approach for understanding motor control. Integrative and Comparative Biology, 47(1), 16–54. https://doi.org/10.1093/icb/icm024

Ortiz, D., Gravish, N., & Tolley, M. T. (2019). Soft Robot Actuation Strategies for Locomotion in Granular Substrates. IEEE Robotics and Automation Letters, 4(3), 2630–2636. https://doi.org/10.1109/LRA.2019.2911844

Pitcher, C., & Gao, Y. (2017). First implementation of burrowing motions in dual-reciprocating drilling using an integrated actuation mechanism. Advances in Space Research, 59(5), 1368–1380. https://doi.org/10.1016/j.asr.2016.12.017

Richefeu, V., El Youssoufi, M. S., & Radjaï, F. (2006). Shear strength properties of wet granular materials. Physical Review E - Statistical, Nonlinear, and Soft Matter Physics, 73(5), 1–11. https://doi.org/10.1103/PhysRevE.73.051304

Roberts, B., Lind, R., & Chatterjee, S. (2011). Flight dynamics of a pterosaur-inspired aircraft utilizing a variable-placement vertical tail. Bioinspiration and Biomimetics, 6(2). https://doi.org/10.1088/1748-3182/6/2/026010

Roubik, K., Sykora, K., Sieger, L., Ort, V., Horakova, L., & Walzel, S. (2022). Perlite is a suitable model material for experiments investigating breathing in high density snow. Scientific Reports, 12(1), 1–12. https://doi.org/10.1038/s41598-022-06015-y

Sadeghi, A., Mondini, A., & Mazzolai, B. (2017). Toward self-growing soft robots inspired by plant roots and based on additive manufacturing technologies. Soft Robotics, 4(3), 211–223. https://doi.org/10.1089/soro.2016.0080

Schiebel, P. E., Astley, H. C., Rieser, J. M., Agarwal, S., Hubicki, C., Hubbard, A. M., Diaz, K., Mendelson, J. R., Kamrin, K., & Goldman, D. I. (2020). Mitigating memory effects during undulatory locomotion on hysteretic materials. ELife, 9, 1–32. https://doi.org/10.7554/eLife.51412

Sharpe, S. S., Kuckuk, R., & Goldman, D. I. (2015). Controlled preparation of wet granular media reveals limits to lizard burial ability. Physical Biology, 12(4), 46009. https://doi.org/10.1088/1478-3975/12/4/046009

Sharpe, S. S., Koehler, S. A., Kuckuk, R. M., Serrano, M., Vela, P. A., Mendelson, J., & Goldman, D. I. (2015). Erratum: Locomotor benefits of being a slender and slick sand-swimmer. Journal of Experimental Biology (Vol. 218, Issue 7, p. 1111). Company of Biologists Ltd. https://doi.org/10.1242/jeb.121939

Shinoda, A., Fujiwara, S. ichi, Niiya, H., & Katsuragi, H. (2018). Void structure stability in wet granular matter and its application to crab burrows and cometary pits. Scientific Reports, 8(1), 1–8. https://doi.org/10.1038/s41598-018-33978-8

Sodeyama, K., Sakka, Y., Kamino, Y., & Seki, H. (1999). Preparation of fine expanded perlite. Journal of Materials Science, 34(10), 2461–2468. https://doi.org/10.1023/A:1004579120164

Stone, M. B., Barry, R., Bernstein, D. P., Pelc, M. D., Tsui, Y. K., & Schiffer, P. (2004). Local jamming via penetration of a granular medium. Physical Review E - Statistical Physics, Plasmas, Fluids, and Related Interdisciplinary Topics, 70(4), 10. https://doi.org/10.1103/PhysRevE.70.041301

Susha Lekshmi, S. U., Singh, D. N., & Shojaei Baghini, M. (2014). A critical review of soil moisture measurement. Measurement: Journal of the International Measurement Confederation, 54, 92–105. https://doi.org/10.1016/j.measurement.2014.04.007

Tang, Y., & Tao, J. (2022). Multiscale analysis of rotational penetration in shallow dry sand and implications for self-burrowing robot design. Acta Geotechnica, 17(10), 4233–4252. https://doi.org/10.1007/s11440-022-01492-x

Tang, Y., Zhong, Y., & Tao, J. (2024). Bio-inspired rotational penetration and horizontal self-burrowing soft robot. Acta Geotechnica, 0123456789. https://doi.org/10.1007/s11440-023-02173-z

Winter, A. G., Deits, R. L. H., Dorsch, D. S., Slocum, A. H., & Hosoi, A. E. (2014). Razor clam to RoboClam: Burrowing drag reduction mechanisms and their robotic adaptation. Bioinspiration and Biomimetics, 9(3). https://doi.org/10.1088/1748-3182/9/3/036009

Wu, N. C., Alton, L. A., Clemente, C. J., Kearney, M. R., & White, C. R. (2015). Morphology and burrowing energetics of semi-fossorial skinks (Liopholis spp.). Journal of Experimental Biology, 218(15), 2416–2426. https://doi.org/10.1242/jeb.113803

Xue, Z., Zhao, C., & Tao, J. (2024). Reducing penetration resistance through bio-inspired head oscillation. IOP Conference Series: Earth and Environmental Science, 1337(1). https://doi.org/10.1088/1755-1315/1337/1/012040

Zhang, D., & Gao, Z. (2012). Forward kinematics, performance analysis, and multi-objective optimization of a bio-inspired parallel manipulator. Robotics and Computer-Integrated Manufacturing, 28(4), 484–492. https://doi.org/10.1016/j.rcim.2012.01.003

Zhang, T., & Goldman, D. I. (2014). The effectiveness of resistive force theory in granular locomotion. Physics of Fluids, 26(10), 1–17. https://doi.org/10.1063/1.4898629

Zagal, J. C., Armstrong, C., & Li, S. (2012). Deformable octahedron burrowing robot. Artificial Life 13: Proceedings of the 13th International Conference on the Simulation and Synthesis of Living Systems, ALIFE 2012, 431–438. https://doi.org/10.7551/978-0-262-31050-5-ch057